2012

Power Control of Diesel Engine-Generator Set Subject to Emission Constraints

Xiaoxi Zhang
University of Windsor

Power Control of Diesel Engine-Generator Set Subject to Emission Constraints

by

Xiaoxi Zhang

A Thesis
Submitted to the Faculty of Graduate Studies
through the Department of Mechanical, Automotive, and Materials Engineering
in Partial Fulfillment of the Requirements for
the Degree of Master of Applied Science at the
University of Windsor

Windsor, Ontario, Canada

2012

Power Control of Diesel Engine-Generator Set Subject to Emission Constraints

by

Xiaoxi Zhang

APPROVED BY:

_____

Dr. Xiang Chen, Co-Advisor
Department of Electrical and Computer Engineering

_____

Dr. Ming Zheng, Co-Advisor
Department of Mechanical, Automotive and Materials Engineering

_____

Dr. Jimi Tjong, Department Reader
Department of Mechanical, Automotive and Materials Engineering

_____

Dr. Xiaohong (Iris) Xu, Outside Reader
Department of Civil and Environmental Engineering

_____

Dr. Behnam Shahrrava, Outside Reader
Department of Electrical and Computer Engineering

_____

Dr. Biao Zhou, Chair of Defence
Department of Mechanical, Automotive and Materials Engineering

January 31, 2012

AUTHOR'S DECLARATION OF ORIGINALITY

I hereby certify that I am the sole author of this thesis and that no part of this thesis has been published or submitted for publication.

I certify that, to the best of my knowledge, my thesis does not infringe upon anyone's copyright nor violate any proprietary rights and that any ideas, techniques, quotations, or any other material from the work of other people included in my thesis, published or otherwise, are fully acknowledged in accordance with the standard referencing practices. Furthermore, to the extent that I have included copyrighted material that surpasses the bounds of fair dealing within the meaning of the Canada Copyright Act, I certify that I have obtained written permission from the copyright owner(s) to include such material(s) in my thesis and have included copies of such copyright clearances to my appendix.

I declare that this is a true copy of my thesis, including any final revisions, as approved by my thesis committee and the Graduate Studies office, and that this thesis has not been submitted for a higher degree to any other University or Institution.

ABSTRACT

Series Hybrid Electric Vehicle (SHEV) is a promising solution to reducing fuel consumption and emissions. It equipped with large battery packs that allow the SHEV first operates in full electrical mode, once the on-board batteries are depleted, the engine generator set turns on to sustain the power demand. Therefore, the efficiency and emissions of a SHEV depend heavily on the operation of the engine generator set. For the simultaneous power and emission control, the model based engine generator set control was developed. Then, emission estimation and Exhaust Gas Recirculation (EGR) model were implemented. The amount of EGR was determined based on the trade-off between NOx and soot emissions. Finally, Model Predictive Control (MPC) was designed and applied to control the power of the engine generator set at its operation point to achieve the best fuel economy as well as to satisfy the power demand.

DEDICATION

To my parents and my wife

ACKNOWLEDGEMENTS

I sincerely thank my supervisors Dr. Xiang Chen and Dr. Ming Zheng. My graduate studies would not have been possible without their patience, guidance and assistance. I would also like to thank my committee members, Dr. Xiaohong Xu, Dr. Behnam Shahrrava and Dr. Jimi Tjong for their valuable advice.

Many thanks also go to my colleagues in the Clean Diesel Engine Laboratory: Dr. Meiping Wang, Dr. Shui Yu, Dr. Usman Asad, Xiaoye Han, Tongyang Gao, Prasad Divekar, Fangfang Lin, Kelvin Xie, Marko Jeftic and last but not least Arturo Mendoza. It was a pleasure to work with everyone.

Furthermore, I gratefully acknowledge the support from Dr. Rochdi Trigui in Transport and Environment Laboratory of French Institute of Science and Technology for Transport, Development and Networks (IFSTTAR).

TABLE OF CONTENTS

LIST OF TABLES

LIST OF FIGURES

LIST OF ABBREVIATIONS

AC	Alternating Current
B	Damping Coefficient
BMEP	Break Mean Effective Pressure
BMS	Battery Management System
BSFC	Brake Specific Fuel Consumption
CO	Carbon Monoxide
CO_2	Carbon Dioxide
C_p	Specific Heat at Constant Pressure
C_v	Specific Heat at Constant Volume
DOE	Department of Energy
DOC	Diesel Oxidation Catalyst
ECU	Engine Control Unit
EGR	Exhaust Gas Recirculation
EMF	Electro Magnetic Field
EPA	Environmental Protection Agency
FSN	Filter Smoke Number

GDI	Gasoline Direct Injection
HEV	Hybrid Electric Vehicle
HRR	Heat Release Rate
I_m	Motor Supplied Current
J	Inertia
k_t	Torque Constant
MPC	Model Predictive Control
m_f	Fuel Injection Quantity Per Cycle
mmf	Magnetomotive Force
$\dot{m}_{ff}$	Fuel Flow Rate
NOx	Nitrogen Oxides
n	Engine Speed
p	Pressure
P	Number of Poles
PM	Particulate Matter
PMSM	Permanent Magnetic Synchronous Machine
PID	Proportional-Integral-Derivative

PWM	Pulse Width Modulation
Q_{LHV}	Lower Heating Value of the Fuel
SOC	State Of Charge
THC	Total Hydrocarbons
T	Torque
V	Volume
V_a, V_b, V_c	A, B, C Three Phase Voltage
V_d, V_q	d-axis and q-axis Voltage
WOT	Wide Open Throttle
i_d	d-axis Current
i_q	q-axis Current
rpm	Revolutions Per Minute
α	Angle Between Rotor Field and Stator Current Phasor
θ	Crank Angle
θ_0	Crank Angle at the Start of Combustion
α_{wall}	Wall Heat Transfer Coefficient
λ_d	Flux in d-axis

λ_q	Flux in q-axis
λ_f	Permanent Magnetic Flux
η_{th}	Thermal Efficiency
ω_r	Rotor Speed
ω_{rated}	Motor Rated Speed
ϑ	Divertive Operator.
γ	Specific Heat Ratio

CHAPTER 1

INTRODUCTION

1.1 Motivations

Driven by the more stringent emission regulations and increasing fuel price, the automotive industry and academia are continuously pursuing new powertrain technologies. SHEV being a member in the HEV family, is a promising alternative solution to meet the requirements of both emission and efficiency. The detailed motivations are illustrated in the following.

Due to the increasing environmental concerns and harmful emissions' impact on health, government authorities enforce aggressive emission standards. Figure 1-1 and Figure 1-2 demonstrate as the aggressive changes in emission standards with time. The US Environmental Protection Agency (US EPA) has implemented stringent diesel emissions standards for 2010 to 2013 that force a drastic reduction in NOx and PM emission levels [2]. The 2010 US EPA diesel emissions standards for on-highway engines imposed emissions reductions by 90% from the 2004 levels, to 0.2 gram per horsepower hour (g/hp-hr) for NOx and 0.01 g/hp-hr for PM.

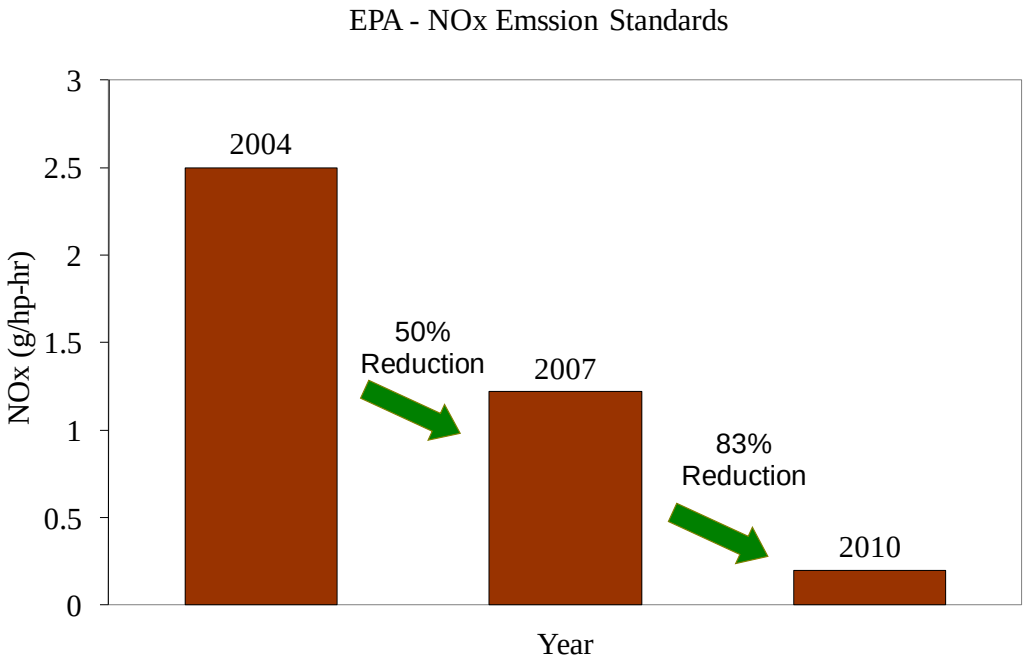

Figure 1-1: EPA Diesel Emission Standards – NOx [2]

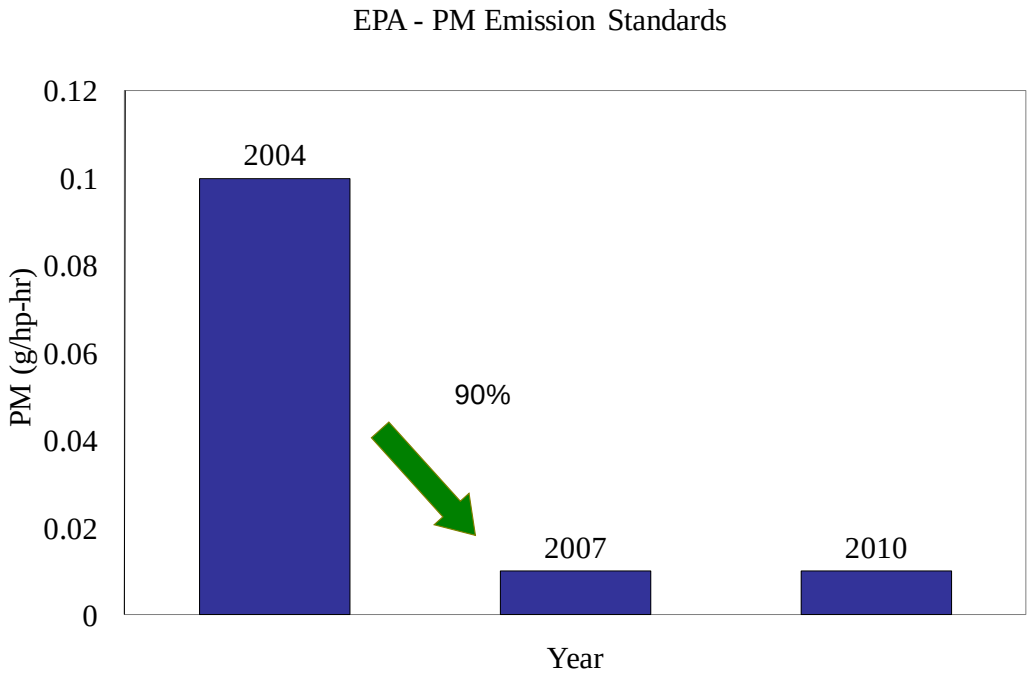

Figure 1-2: EPA Diesel Emission Standards – PM [2]

Figure 1-3 shows the European Emission Standards over the years [3]. In Europe, the upcoming Euro VI emission standards requires as a 75% reduction in NOx emission compared to the Euro V standards in 2008, moreover a 50% reduction has to be achieved for PM by the Euro VI emission standards. Automobile manufacturers are not allowed to sell vehicles without facing an environmental penalty, if these regulations are not met. Vehicular emission improvements must be considered in the design and engineering stage of vehicles.

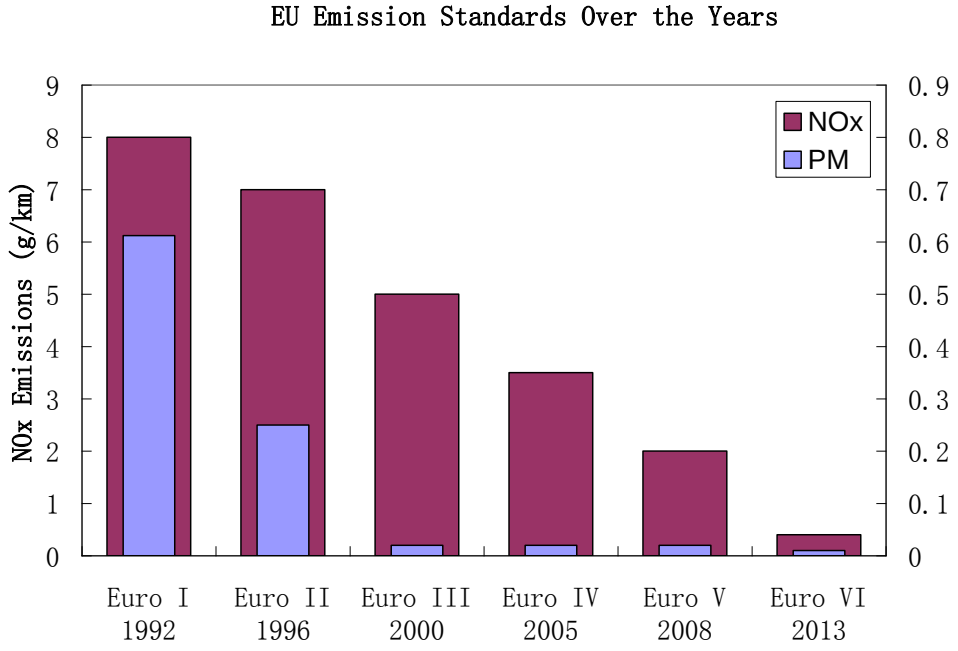

Figure 1-3: European Emission Standards 1992 - 2013 [3]

The second motivation of this research comes from the need for improving vehicle efficiency. Global efficiency regulations and increasing fuel prices are expected to continuously demand improved vehicle fuel efficiency. Transportation sector consumes a

large portion of the total crude oil production. The US Department of Energy (DOE) states that over 15 million barrels of crude oil are being consumed by the transportation sector which accounts for 69% of the total consumption nationwide [4]. Other studies indicate that the transportation sector performed the worst overall in energy conversion efficiency estimated at only 20% [5]. As a result, intensive fuel efficiency improvements are necessary for both near-term and long-term.

In many countries, fuel efficiency targets are being enforced by government authorities. Figure 1-4 show the EPA and European fuel economy targets respectively [6]. The EPA requires an overall 17% improvement of efficiency over the current efficiency level for both passenger car and light truck by the year 2016. European efficiency targets are extremely challenging, especially for the 2020 target which require a 50% efficiency improvement over the current average as shown in Figure 1-5 [7].

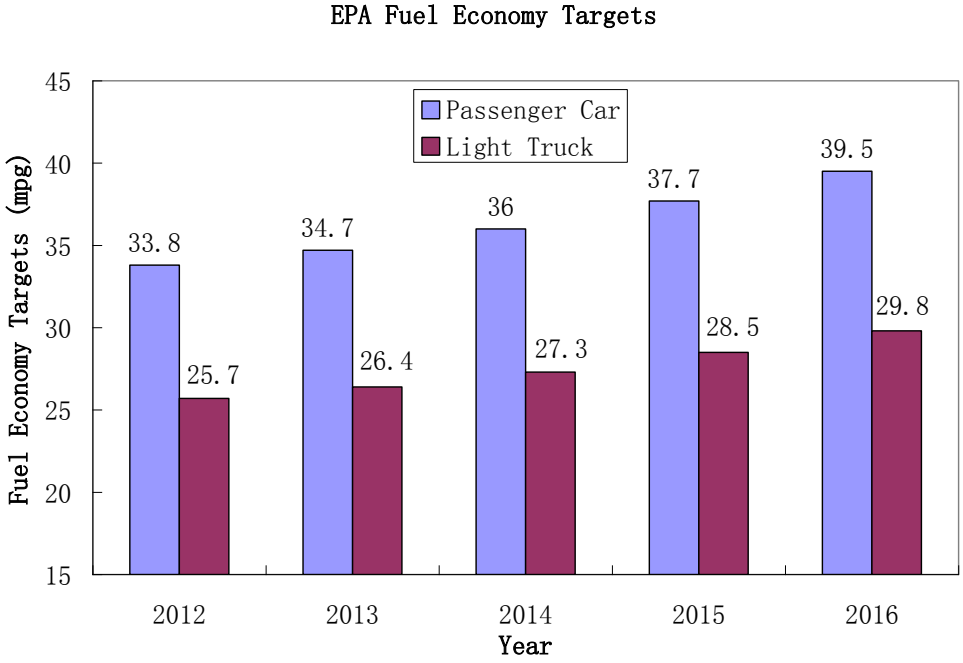

Figure 1-4: EPA Fuel Economy Targets

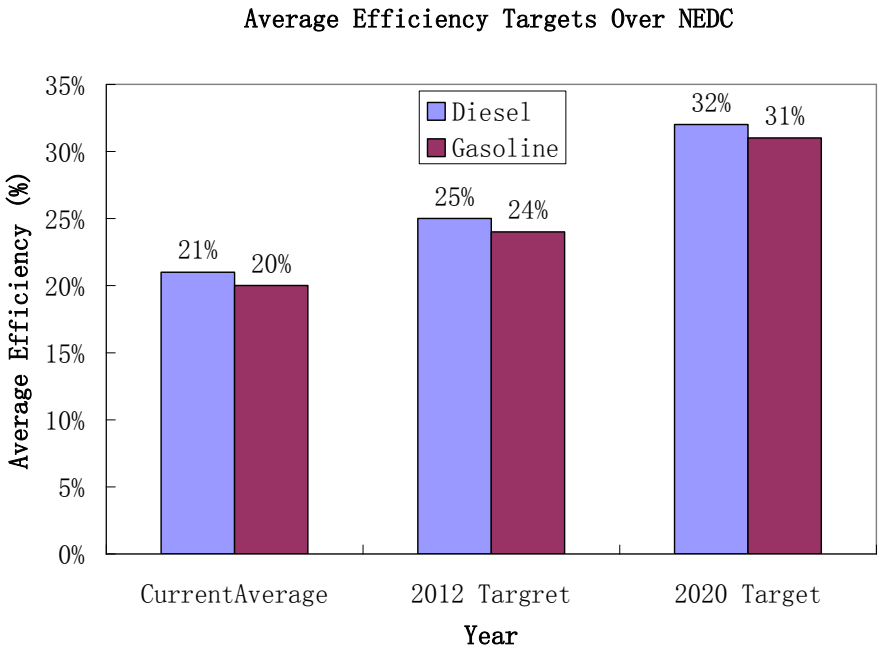

Figure 1-5: Average Efficiency Targets over NEDC

As a result, the automotive industry is constantly pursuing technologies to reduce the dependency of transportation on petroleum fuel and to improve the vehicle efficiency. In the past decade, the Hybrid Electric Vehicle (HEV) has successfully demonstrated to be a viable technology to save fuel and reduce emissions, through the synergy of internal combustion engine and electric machines. Many HEVs reported a 20% to 40% fuel economy improvement compare to the current conventional vehicles [8]. Series hybrid electric vehicle (SHEV) is a member of the HEV family, equipped with larger battery, it can store enough on-board electrical energy to satisfy the daily commute range of an average driver without turning on the engine, providing even better fuel efficiency and less emissions than standards HEVs. Many automotive companies like GM, TOYOTA, VOLVO and BMW have announced the SHEV prototypes. SHEV can be an effective solution to change people's transportation in the near future. The engine generator set is

one of the most critical units in a SHEV. In order to have acceptable overall vehicle performance and emissions, its power control issues and emissions should be well addressed. This study will focus on the lower level component of SHEV: engine generator set power and emission control, which act as the foundation of the further system level clean diesel SHEV project.

1.2 Research Objectives

Previous Engine Generator-Set studies are typically focused on improving fuel economy rather than emissions [1-3] for HEV applications. This research intends to consider both fuel economy and emissions control of engine generator set for a SHEV application.

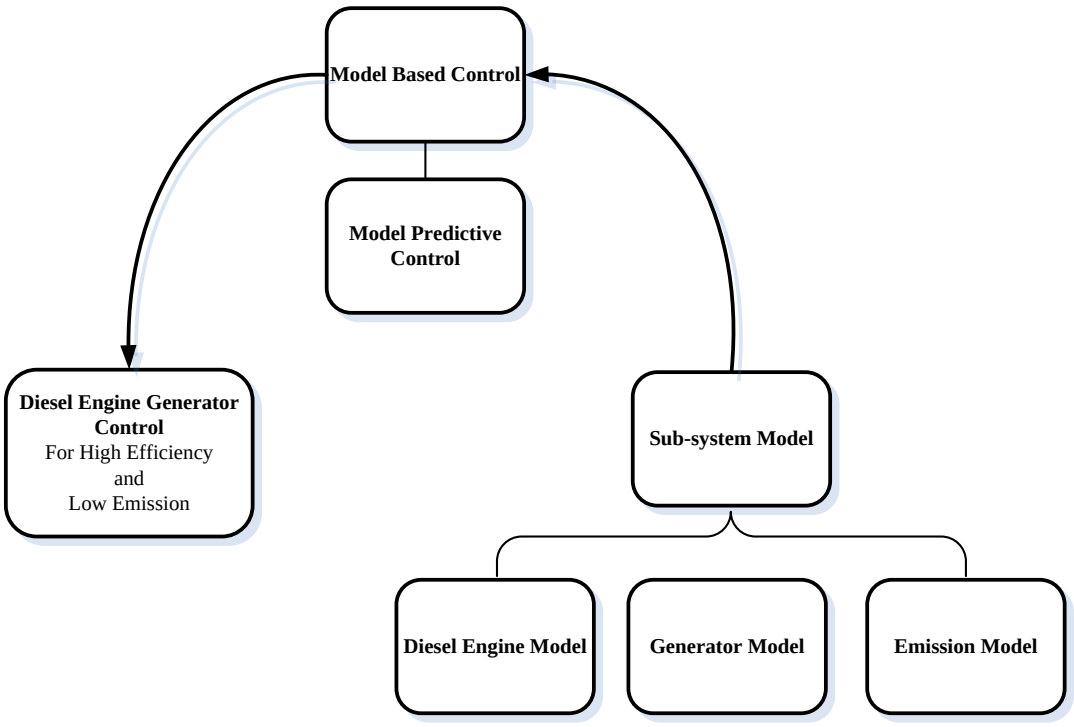

Figure 1-6: Research Outline

The objectives of this research are identified as the following, shown in Figure 1-6:

- To develop a diesel engine generator set model, which can be used as a platform to evaluate the system performance and energy flow.

- To implement a power controller for the engine generator set to govern the operation at its high efficiency operating points, and to enable variable speed operation according to the vehicle power demands.

- To implement an emission model to predict major diesel exhaust emissions such as NOx and soot. Furthermore, NOx and soot should be controlled by one of the major emission measures, EGR. The EGR amount will be determined to achieve an effective reduction in NOx emission, while controlling the trade-off between NOx and soot, and keeping soot emission at an acceptable level.

Figure 1-7 shows an overview of the control architecture of the clean diesel SHEV project. The major energy storage system includes the battery and super capacitors.

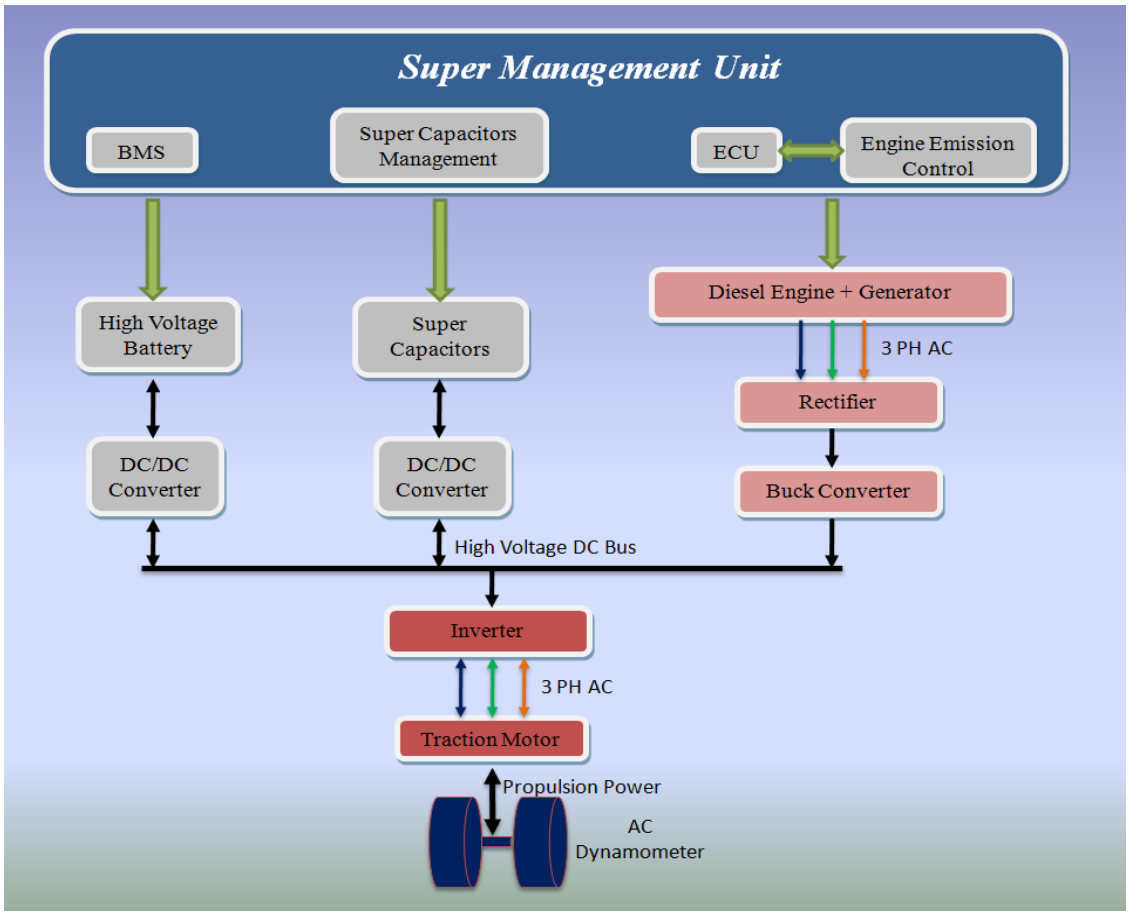

Figure 1-7: Clean Diesel SHEV Powertrain System Overview

The onboard electric energy provided by the engine generator set, traction motor supplies the drive torque. A tremendous amount of research can be done to improve overall vehicle efficiency, performance and emissions. However, it requires the lower level components and controllers to be well designed and capable of achieving the required performance. The engine generator set is an important powertrain unit in SHEV. Vehicle emissions and fuel efficiency highly depend on its operation. The operation and control associated with this unit should be well addressed.

CHAPTER 2

REVIEW OF LITERATURE

2.1 Series Hybrid Electric Vehicle

Since the invention of Internal Combustion (IC) engine, IC engines have undergone evolutionary improvements in terms of fuel efficiency, emission reductions and control. In a conventional vehicle, the engine operates all speed ranges and has to meet all of the vehicle's power demands. However, an engine can only provide the maximum efficiency and low emissions for a small range of speed and load points. Therefore, IC engines suffer fuel inefficiency and higher emissions in real world driving situations. The automotive industry is continuously improving current engine technologies and pursuing alternative powertrain technologies for higher efficiency and lower emissions. HEV is one of the viable technologies.

In 1997, Toyota released the first global-scale passenger HEV. HEV is drawing a significant amount of attention and research due to its capabilities to demonstrate its efficiency and emission reduction. Depending on how the power is supplied to the drive train, HEVs can be classified as three main categories: series, parallel and series-parallel [11]. SHEV is the simplest form of general hybrid vehicles. It is equipped with larger battery packs, which are capable of being charged by an electrical grid. The SHEV intends to operate mainly as an electric vehicle to satisfy the average person's daily commute distance. This way, the SHEV can take the advantage of the inexpensive grid electricity in comparison to the costs of gasoline or diesel. Once the battery reaches the

lower battery state of charge (SOC) threshold, an on board engine generator will be turned on to sustain the battery charge and serve as a ‘range extender’ [12, 13].

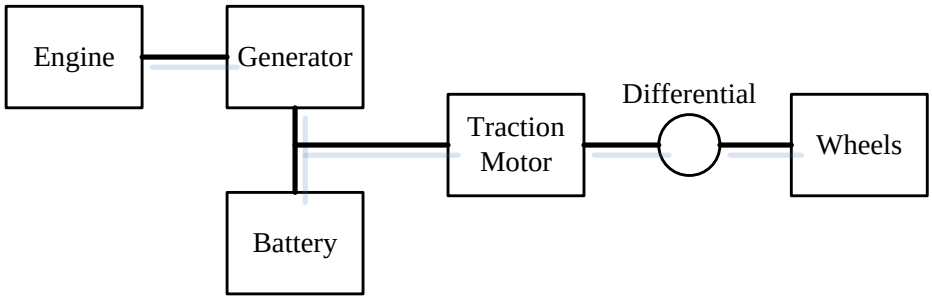

Figure 2-1: A SHEV Configuration

The SHEV has the simplest configuration of all. The engine has no physical connection to the drivetrain; the traction motor is the energy converter to provide propulsion power as shown in Figure 2-1. Unlike the IC engine in a conventional vehicle which is designed to operate over a wide variety of power demands and operating conditions, the SHEV engine operation region is independent of vehicle velocity. As a result, it gives the possibility for optimal operation. Since the electric motor provides the traction force, the drivability and performance of the vehicle primarily depends on the specifications of the traction motor. Hence, often the IC engine can be downsized to the average vehicle power demand in a series HEV. Once the battery has been depleted, the engine generator set starts to generate power. The overall efficiency of A SHEV could be less when compared to other configurations due to the energy conversion lost from mechanical to electrical then back to mechanical. However the cost, the simplicity of the design, the less complicated system control strategies and easy maintenance are the advantages of this configuration [13, 14].

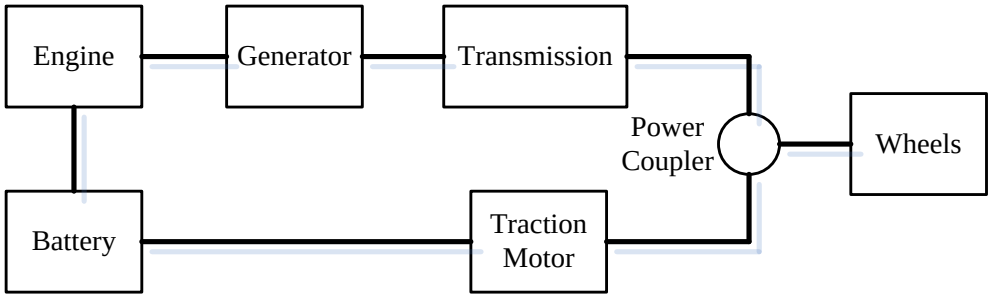

Figure 2-2: A Parallel HEV Configuration

A layout of a Parallel HEV is shown in Figure 2-2. Unlike the SHEV configuration both engine and traction motor serve as propulsion power sources. The engine is mechanically coupled to the generator and it assists the traction motor to contribute traction torque as well. However, it requires sophisticated transmission for multiple power sources coupling. Furthermore, the vehicle level power control is more complex than SHEV.

The engine requirements and operation in a SHEV is vastly different from the one in a typical vehicle. Engine friction and heat loss are the two major losses of an IC engine. Heat loss increases with decreasing engine speed and friction loss increases with increasing engine speed. An IC engine is more efficient operating at a relatively high load at any speed and operation at mid-speed ranges (about 50% of the top engine speed) gives the best overall efficiency where the balance of friction and heat loss is obtained. In a SHEV, the engine is isolated from fluctuating power demand. Since the traction motor is providing the driving traction, the engine can avoid running at a low efficiency range but remain running at a high efficiency range [15].

In a SHEV, the engine can be downsized. With the assistance of the battery and traction

motor, the engine can be selected to just meet the average power demand, thus making it unnecessary to provide the vehicle peak power demand. Fuel efficiency will be improved from reduced engine friction while the engine operates at a higher load. The engine friction is proportional to the engine displacement; smaller engines will encounter less friction during operation. For the same engine power outputs, an engine running at a higher load is more efficient. With a downsized engine, the size and mass of the engine is also reduced.

In a SHEV, fuel saving can still be achieved from the vehicle start-stop and regenerative braking typical for an HEV platform. In a real world driving scenario, the engine can be turned off while the vehicle idles and coasts down from a higher speed. Regenerative braking can be achieved through the recycling of mechanical energy to electrical energy by the traction motor to charge the battery.

2.2 Diesel Engine Generator Set Control

A diesel engine generator set that consists of a diesel engine directly coupled to a generator was designed to provide enough electrical power for steady state operation. For a stationary application, the engine generator set is commonly operated at a fixed speed. For applications in HEV, variable speed operation of the engine generator set has been proven to improve fuel efficiency and system response. [16]

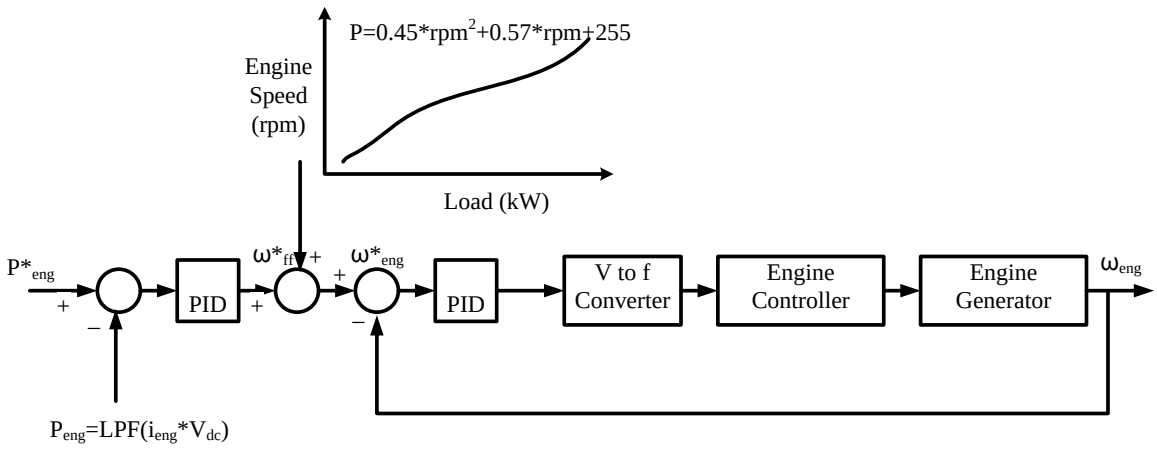

Figure 2-3: Power Control Block Diagram of the Engine (Adapted From [17])

Figure 2-3 shows the current power control block diagram of the engine generator set [17]. The power level of the engine generator set was controlled by adjusting the engine speed. The engine governor controller uses a servomotor to electromechanically control the engine throttle angle. This governor translates the demanded speed signal into a pulse width modulation (PWM) signal used in the servomotor throttle. To obtain the relationship between the engine speed and the engine generator set power output, the unit was installed on a test bed to monitor and record the engine speed at several points from no-load to the full-load condition while maintaining a constant terminal voltage at the system dc-link value throughout the tests. Then a second order approximation was used to fit to these speed and load points from the tests. This second-order approximation was also used as feed forwarding the engine speed corresponding to the required power output. PID controllers are used to regulate engine speed to the reference [17].

There are two main improvements that can be made from the current approach. The low order approximation used to describe the engine speed and power relationship can be a source of error. The operation of the engine and generator are highly nonlinear. The

approximation is used to determine engine reference speed to rotate the generator to meet the power demand. If the approximation is not adequate to describe the engine speed and power relationship, the engine generator can be either not producing enough power or generating extra power resulting in unnecessary high fuel consumption.

PID controllers are applied to regulate engine speed to the reference. Besides the popularity of PID, it requires significant amount of effort to tune in to the optimized parameters; In addition, it lacks of predicting feature, which is inadequate to provide satisfied response. Using another controller such as Model Predictive Control (MPC) to replace PID can be another improvement from the control perspective.

2.3 Diesel Engine Emissions and Emission Control

On a SHEV, the engine generator set generates electricity on-board once the battery is depleted. It is also the emission source. In order to control emissions, it is necessary for engine emissions to be understood.

Emission standards regulate the amount of NOx, THC, CO and PM in general. Due to its lean burn characteristics, a diesel engine produces a low amount of CO and THC but high levels of NOx and PM among the emissions. Moreover, THC and CO can be reduced by over 70% with the help of a low cost and effective Diesel Oxidation Catalyst (DOC) [18]. This leaves NOx and PM challenged to meet the diesel emission standards. In this research, the focus will be on NOx and PM emissions control. The production of NOx from engine combustion depends on the amount of oxygen available and the combustion

temperature. The NOx formation rate increases vastly as the combustion temperature moves beyond 1800 degree K [19]. NOx impacts both the environmental and health. A portion of nitrogen dioxide reacts with moisture in the atmosphere and is then converted to nitric acid (HNO3) which is the source of acid rain. In the presence of heat and sunlight, ground level ozone is formed when NOx and volatile organic compounds react. Children, the elderly and people with lung diseases such as asthma are at risk due to the adverse effects of ozone. NOx can react with ammonia, moisture, and other compounds to form small particles. These harmful particles can penetrate into the lungs and cause respiratory disease. As a result, the amount of NOx emission should be strictly limited.

Diesel PM is also referred to as diesel soot. It is the term for very fine particles solid or liquid which are composed of a carbon and ash covered by organic compounds, sulphates and nitries and metals. Diesel PM is a health concern, as it can be inhaled by human lungs and, resulting in damages to the respiratory systems.

Over recent decades, diesel engines have become cleaner with the help of both in-cylinder and after treatment emission reduction measures. EGR is known to be one of the most effective NOx reduction methods. It can significantly change the intake heat capacity and reduce the intake oxygen level, resulting in a lower combustion temperature leading to a reduction in NOx [19, 20, and 21]. However, soot increases with a higher rate of EGR, so the amount of EGR is limited by high soot emissions in the conventional diesel combustion.

CHAPTER 3

DESIGN AND METHODOLOGY

3.1 Diesel Engine Model

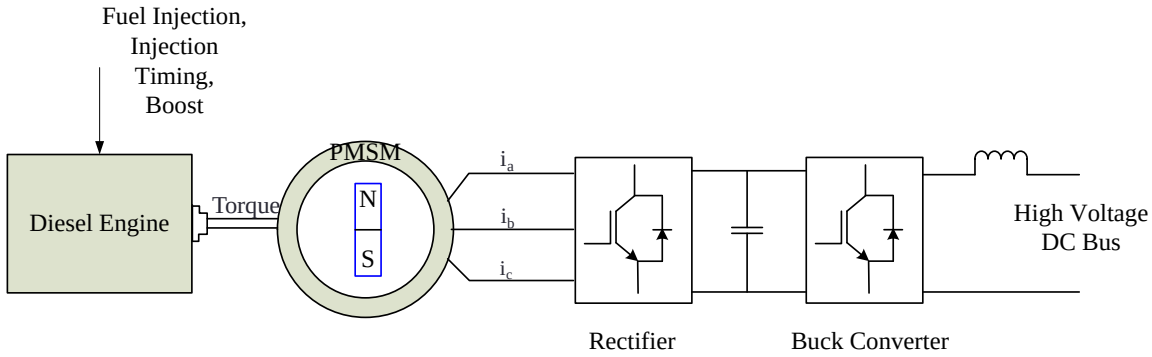

Figure 3-1: Schematic Diagram of Diesel Generator Set

Figure 3-1 shows the schematic diagram of a diesel generator set. The modeling process of the diesel engine and generator are demonstrated.

There are many existing approaches toward diesel engine modeling. The processes in the diesel engine combustion are very complex due to its naturally transient and heterogeneous characteristics [22, 23 and 24]. The selection of these approaches depends on the modeling purpose and the requirement of their accuracy. For control purposes, as well as enable prediction of power and energy flows for the fuel economy evaluation, a simple engine power and fuel economy model based on empirical tests is chosen in this research. Other engine dynamics, such as intake manifold charging, exhaust flow and combustion dynamics are neglected for model simplicity and low computational complexity.

SMART CAR CDI ENGINE

High specific power and power density are desired from an engine generator set so that the power requirements of the SHEV are met while minimizing the size and weight. The engine is used specifically as a range extender to drive the generator rather than as a primary power source. A smaller, lighter and more fuel efficient engine can be used. The engine selected for this research is a diesel engine used in Smart Fortwo vehicle as shown in Figure 3-2. This engine is able to provide exceptionally good fuel economy at 3.3 liters (NEDC test cycle) per 100 kilometers and CO2 emissions of just 88 grams per kilometer in the original vehicle, it has the lowest CO2 emissions in the current production car worldwide [25]. It is also the smallest common rail direct injection diesel engine that features a turbo charger to enhance its fuel economy. This engine was chosen to build a future SHEV powertrain platform in the Clean Diesel Laboratory due to its compact size, high efficiency and the advanced technologies implemented. The detailed engine specifications are listed in Table 3-1.

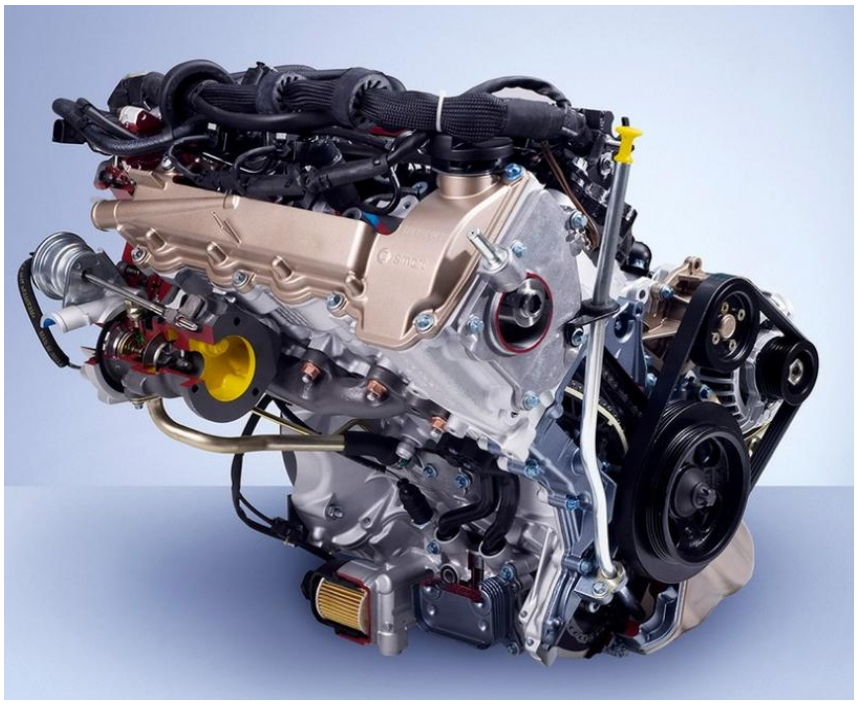

Figure 3-2: Smart Car Cdi Engine

Table 3-1: Smart Cdi engine Specifications

Engine type	3 cylinder, 4 stroke Diesel
Displacement	0.8 liter
Rated Engine Speed	3500 rpm
Compression Ratio	18.5 : 1
Rated Power(peak)	45 HP
Rated Torque	95 lb-ft
Combustion System	Direct injection
Fuel Injection System	Common Rail High Pressure

The smart diesel engine mapping was obtained through experiments in steady state conditions on the test bench in INRETS, France while fuel consumption, engine speed and output torque were recorded. The steady state fuel consumption map does not represent the dynamic behavior of the engine. The recorded points cover the entire working range of the engine. A program has been developed in Matlab to create a plot of engine fuel consumption and the energy conversion efficiency according to functions of the engine speed and engine brake torque in Figure 3-3.

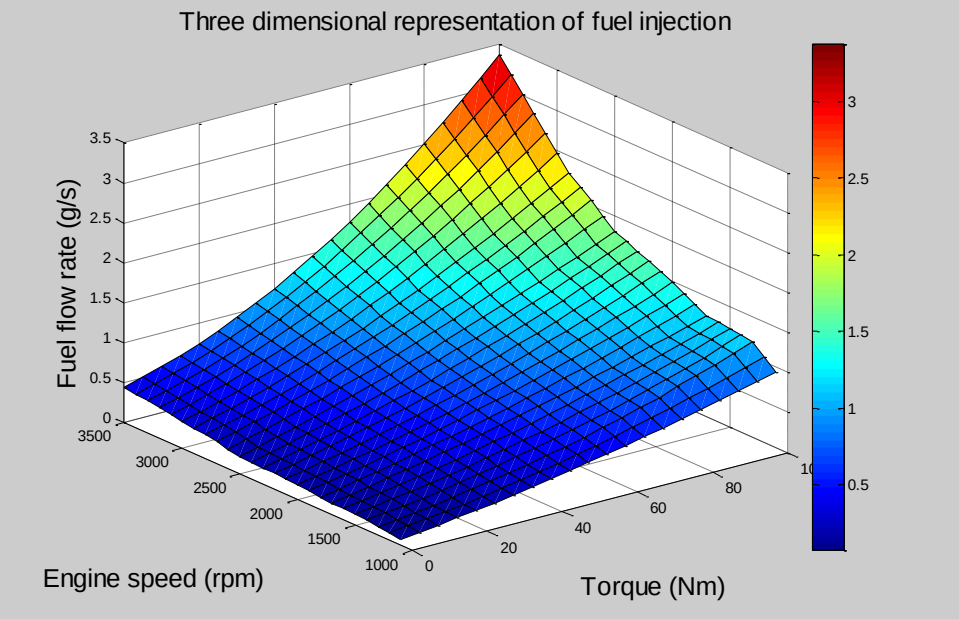

Figure 3-3: Three Dimensional Representation of Fuel Injection

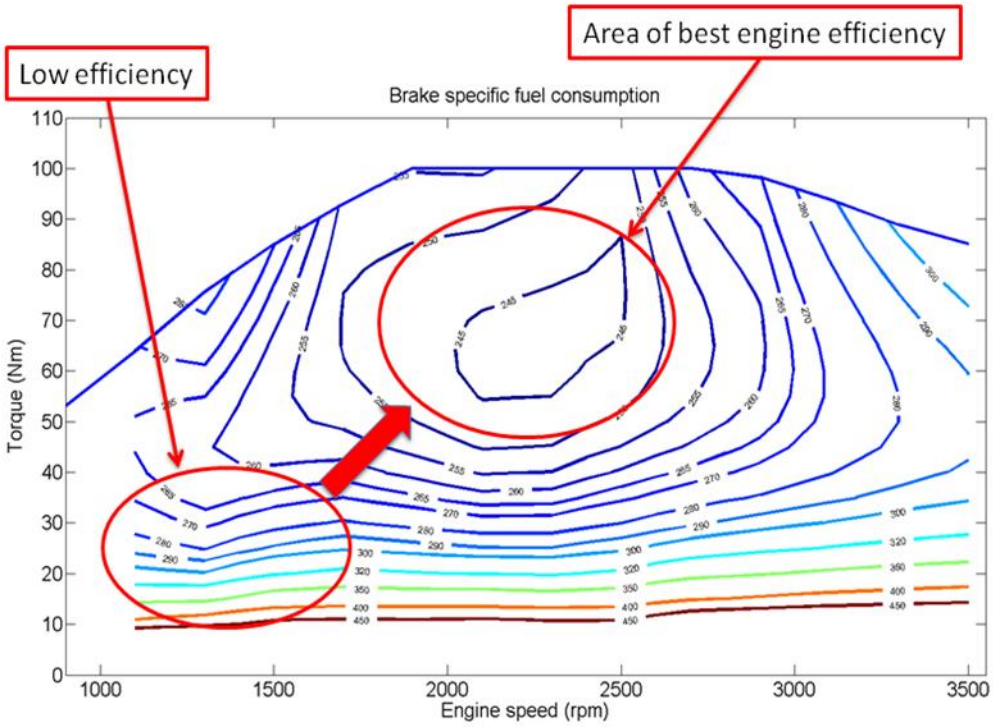

Figure 3-4: Engine Brake Specific Fuel Consumption Contour

The top curve in Figure 3-4 shows the maximum torque output versus engine speed at wide open throttle (WOT). These contours which under the torque curve are brake specific fuel consumption (BSFC) contours with a unit of g/kWh. BSFC is an indication of how efficient an engine is using the fuel supplied to produce mechanical work. It is defined as the ratio of the rate at which fuel is flowing into the engine to the brake horsepower being generated. BSFC allows the fuel efficiency of different engines to be directly compared [15]. The lower the BSFC number, the more efficiently the engine is operating. Under the highlighted area in Figure 3-4, the highest BSFC indicates the best overall efficiency resulting from the balance of friction and heat loss.

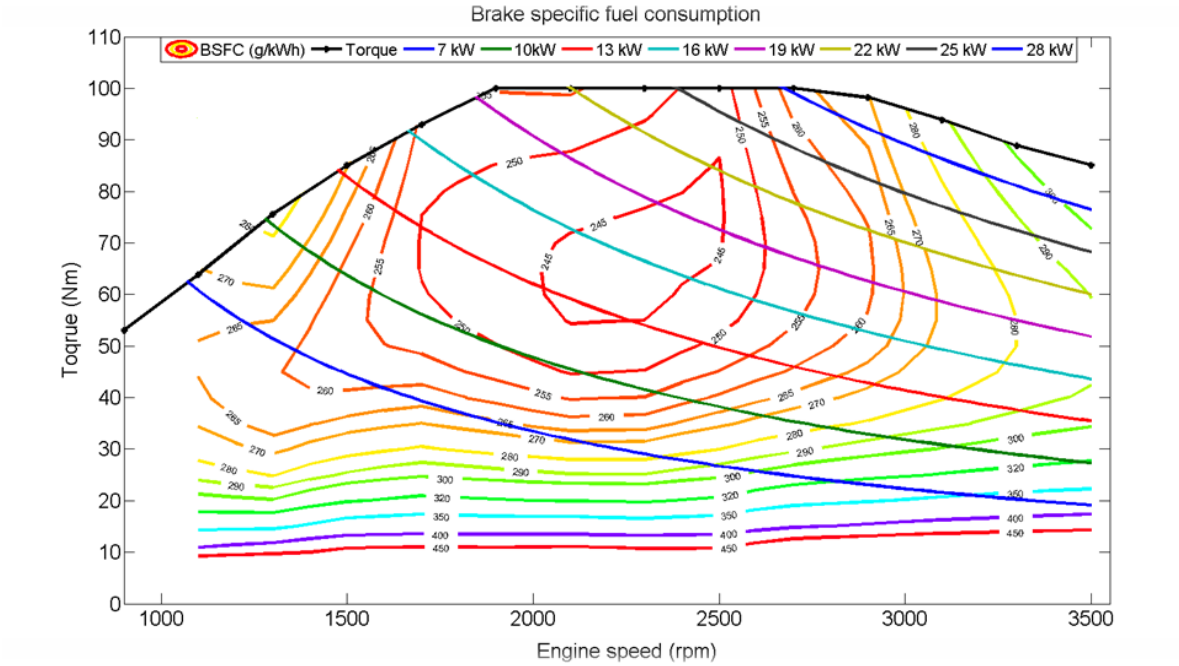

Figure 3-5: Engine BSFC and Power Contour

Engine power output depends on torque and engine speed. The equation to calculate power is shown as:

$$Power(kW) = 2\pi nT / 60 / 1000 \qquad \textbf{3-1}$$

Where n is the engine speed, T is the engine torque.

The engine should provide the power level demanded by the driver as efficiently as possible. In other words, minimize fuel consumption at a driver commanded power level. In a SHEV, and while the hybrid is functioning, the engine should avoid the dynamic operation and keep at steady speed to obtain best emission and fuel consumption [26, 27]. Then the BSFC contours are overlaid with eight different constant engine power lines. These power lines are 3 kW apart from each other and covered the entire engine power

output range from 7 kW to 28 kW as shown in Figure 3-5. Any combination of torque and rpm along the constant lines will produce a constant power output; however engine efficiency varies along the same power line. To achieve high engine efficiency, the engine should operate at its engine optimal operating line. The engine optimal operating line is a sequence of intersections along the constant engine power lines with the peak efficiency contours or the lowest fuel consumption curves if efficiency is the only concern. The red line that connects the blue dots shown in Figure 3-6 is the optimal engine operating line.

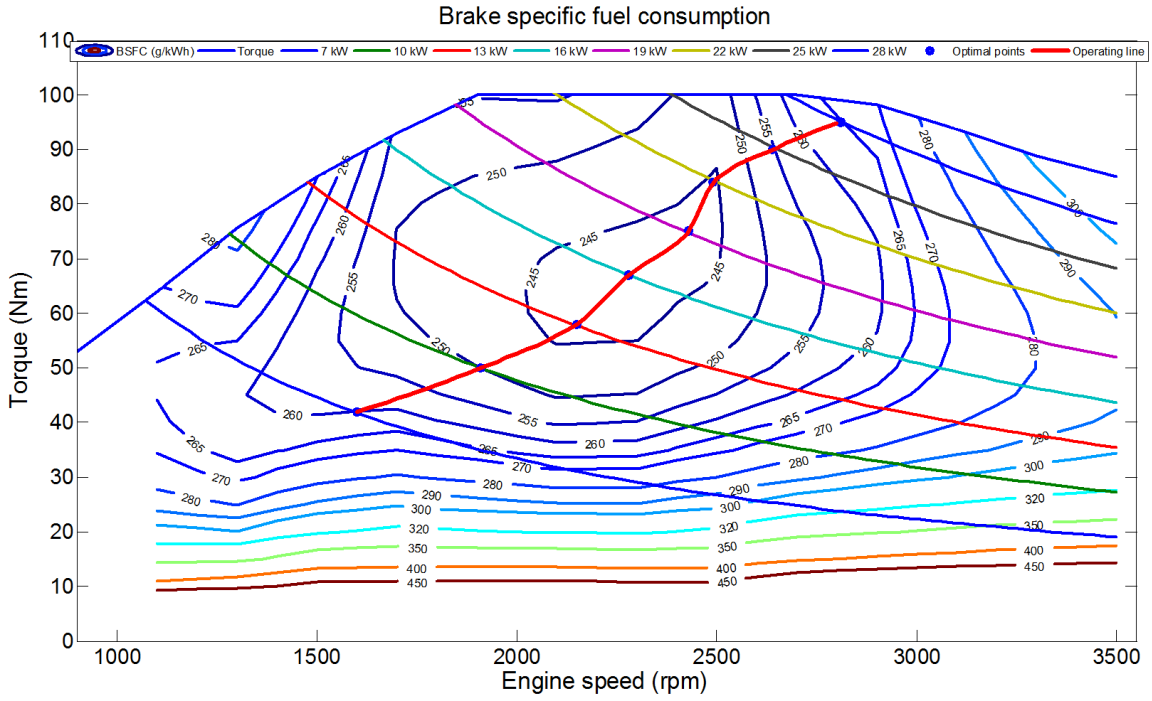

Figure 3-6：Optimized Engine Operation Line

Table 3-2 lists all the engine operation points which were chosen for the engine generator set. Depending on the vehicle power demand, the engine controller will select the corresponded operating point.

Table 3-2: Engine Operation Points

Operating point	Engine speed	Torque	Power	Fuel injection
Units:	rpm	(Nm)	(kW)	(g/s)
#1	1600	42	7	0.508
#2	1950	51	10	0.719
#3	2150	58	13	0.886
#4	2250	67	16	1.07
#5	2450	75	19	1.306
#6	2570	82	22	1.524
#7	2630	90	25	1.749
#8	2800	95	28	2.04

3.2 Permanent Magnetic Synchronous Machine Model

A permanent magnet synchronous motor (PMSM) was chosen as a generator for this research. PMSM can be characterized as having the properties of both the AC induction motor and the brushless DC motor (BLDC). PMSM uses permanent magnets to produce the air-gap magnetic field rather than using electromagnets. These motors are increasingly used in low and mid power applications such as traction motor or generator in HEVs, aerospace, robotics and adjustable speed drives. However, their stator structure

resembles that of an AC induction motor, where the windings are constructed to produce a sinusoidal flux density in the air-gap of the machine. As a result, they perform best when driven by sinusoidal waveforms. However, unlike their AC induction motor counterparts, PMSM motors perform poorly with open-loop scalar control, since there is no rotor coil to provide mechanical damping in transient conditions. Field Oriented Control is the most popular control technique used with PMSM. As a result, torque ripple can be extremely low, on par with that of an AC induction motor. The power density of the permanent magnet synchronous motor is higher than that of the induction motor with the same ratings, as there is no stator power dedicated to the magnetic field production [28, 29, 30 and 31]. Power output of the generator tends to increase as its rotational speed increases. It also increases with larger volume and mass. For a given generator with fixed volume and mass, the faster it spins the more power it produces.

The diesel engine is directly coupled to the generator and the voltage and current of the generator is rectified then supplied to the high voltage bus. The detailed modeling of voltage and current production are shown as follows. The d-q model has been developed on a rotor reference frame as shown in Figure 3-7. At any time, the rotating rotor d-axis makes an angle θ_r with the fixed stator phase axis and rotating stator magnetomotive force (mmf) makes an angle α with the rotor d-axis. Stator mmf rotates at the same speed as that of the rotor.

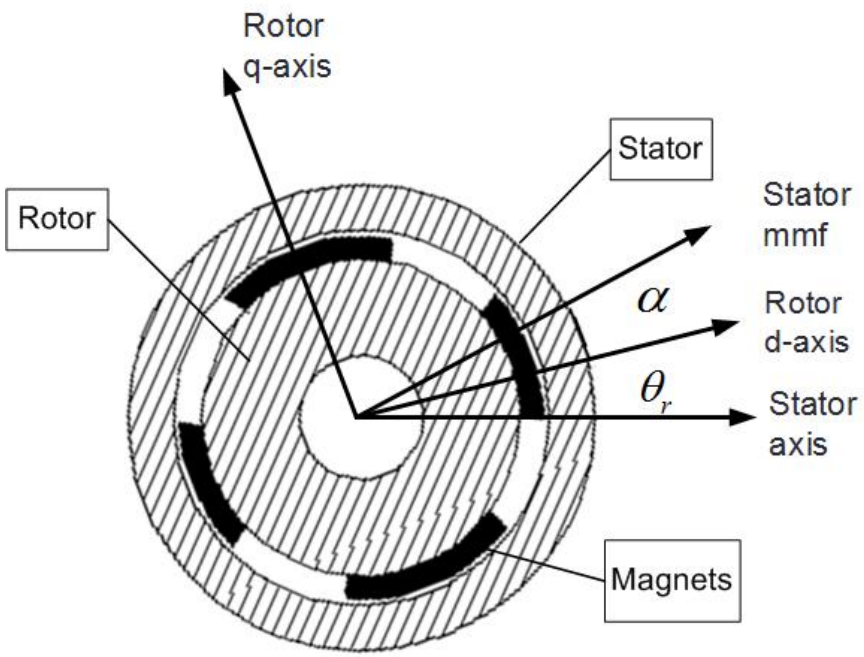

Figure 3-7: PMSM Rotor Axis

The following fundamental assumptions are made regarding the PMSM model:

- No damper winding
- Saturation is neglected
- The induced EMF is sinusoidal
- Eddy currents and hysteresis losses are neglected
- No field current dynamics

Voltage Equations are:

$$V_q = R_s i_q + \omega_r \lambda_d + \vartheta \lambda_q \qquad \textbf{3-2}$$

$$V_d = R_s i_d - \omega_r \lambda_q + \vartheta \lambda_d \qquad \textbf{3-3}$$

R_s is the stator resistance, i_q and i_d are the q-axis current and d-axis current, λ_q and λ_d are the q-axis and d-axis flux linkage. ϑ is the divertive operator.

Flux Linkages are:

$$\lambda_q = L_q i_q \quad \textbf{3-4}$$

$$\lambda_d = L_d i_d + \lambda_f \quad \textbf{3-5}$$

Substituting flux linkages equations into voltage equation

$$V_q = R_s i_q - \omega_r (L_d i_d + \lambda_f) + \vartheta L_q i_q \quad \textbf{3-6}$$

$$V_d = R_s i_d - \omega_r \lambda_q + \vartheta (L_d i_d + \lambda_f) \quad \textbf{3-7}$$

The developed motor torque is given by:

$$T_m = \frac{3}{2}(\frac{P}{2})(\lambda_d i_q - \lambda_q i_d) \quad \textbf{3-8}$$

where P is the number of poles of PMSM.

The mechanical torque equation is

$$T_m = T_L + B\omega_m + J\frac{d\omega_m}{dt} \quad \textbf{3-9}$$

For motor transient and steady response study, dynamic d-q-o modeling is required. Since rotor d-q-o axis is an imaginary coordinate system, it has no direct way to trace and track d-q axis flux and current. So that motor stator phase voltages and currents should be related to the rotor d-q-o axis by using Park transformation. Park transformation is a mathematical transformation used to simplify the analysis of three-phase circuits. To convert the phase variables abc to dqo variables in rotor reference frame, the following

equations can be used

$$P = \frac{2}{3}\begin{bmatrix} \cos(\theta) & \cos(\theta - \frac{2\pi}{3}) & \cos(\theta + \frac{2\pi}{3}) \\ \sin(\theta) & \sin(\theta - \frac{2\pi}{3}) & \sin(\theta + \frac{2\pi}{3}) \\ \frac{1}{2} & \frac{1}{2} & \frac{1}{2} \end{bmatrix} \qquad \textbf{3-10}$$

To convert the dqo to abc variables, the following equations can be used

$$P^{-1} = \begin{bmatrix} \cos(\theta) & \sin(\theta) & 1 \\ \cos(\theta - \frac{2\pi}{3}) & \sin(\theta - \frac{2\pi}{3}) & 1 \\ \cos(\theta + \frac{2\pi}{3}) & \sin(\theta + \frac{2\pi}{3}) & 1 \end{bmatrix} \qquad \textbf{3-11}$$

The current of the motor and three currents of a-b-c axis can be derived from its dynamic model:

$$\begin{aligned} i_a &= I_m \sin(\omega_r t + \alpha) \\ i_b &= I_m \sin(\omega_r t + \alpha - \frac{2\pi}{3}) \\ i_c &= I_m \sin(\omega_r t + \alpha + \frac{2\pi}{3}) \end{aligned} \qquad \textbf{3-12}$$

where, α and ω_r are the angle between rotor field and stator current phasor and rotor angular speed respectively.

Using Park's transformation, the previous currents obtained are the stator currents that can be transformed to the rotor reference frame with the rotor speed. For a given load torque, the q and d axis currents are constants in the rotor reference frames since α is a constant. The q axis current is directly related to the torque production of the motor and

the d axis current is the flux producing component of the stator current.

$$i_q = I_m \sin\alpha \qquad \textbf{3-13}$$

$$i_d = I_m \cos\alpha \qquad \textbf{3-14}$$

Finally the electromagnetic torque equation can be obtained:

$$T_e = \frac{3}{2} P \left[\frac{1}{2} (L_d - L_q) I_m^2 \sin 2\alpha + \lambda_m I_m \sin\alpha \right] \qquad \textbf{3-15}$$

The equivalent circuit of PMSM is shown in Figure 3-8.

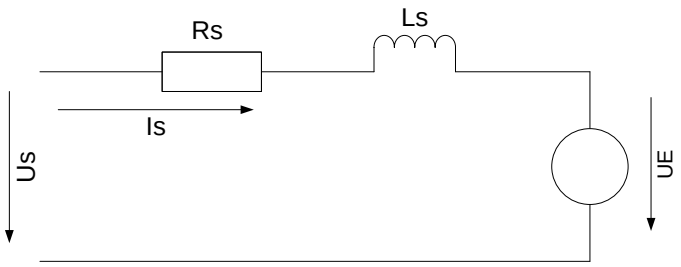

Figure 3-8: Equivalent circuit of PMSM

For small high speed generators round rotors are often used. This application is more interested in the constant torque operation of the generator. Figure 3-9, in constant torque zone where the d-axis and q-axis inductances are equal, so that $L_d = L_q$. α, the angle between rotor field and stator current phasor is 90^o, sinα=1.

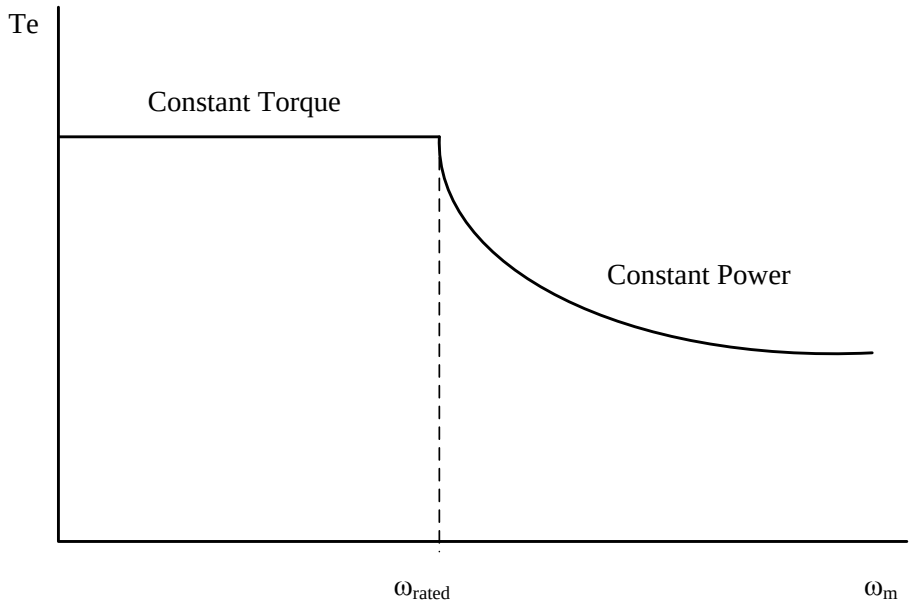

Figure 3-9: Constant Torque and Constant Power of Synchronous Motor

Equation 3-15 can be obtained as follow in the simplified form:

$$T_e = \frac{3}{2} P \lambda_m I_m \qquad \textbf{3-16}$$

Current is related to i_d and i_q,

$$I_m = \sqrt{i_q^2 + i_d^2} \qquad \textbf{3-17}$$

The supply current is equal to torque producing current i_q, and i_d is equal to zero.

Field flux is equal to motor inductance and field current

$$\lambda_f = L_m \cdot i_{fd} \qquad \textbf{3-18}$$

Substituting equation 3-18 and 3-17 into 3-16, electrical torque is obtained as

$$T_g = \frac{3}{2} P \lambda_m i_q \qquad \textbf{3-19}$$

The equations of the system were implemented in Simulink to perform the simulation of the generator system dynamics in Figure 3-10. Simulink is a toolbox extension of the MATLAB program. It is a program for simulating dynamic systems [13]. Simulink has the advantages of being capable of computing complex system dynamics, and provides graphical user interface with visual real time programming and large selection of tool boxes [32].

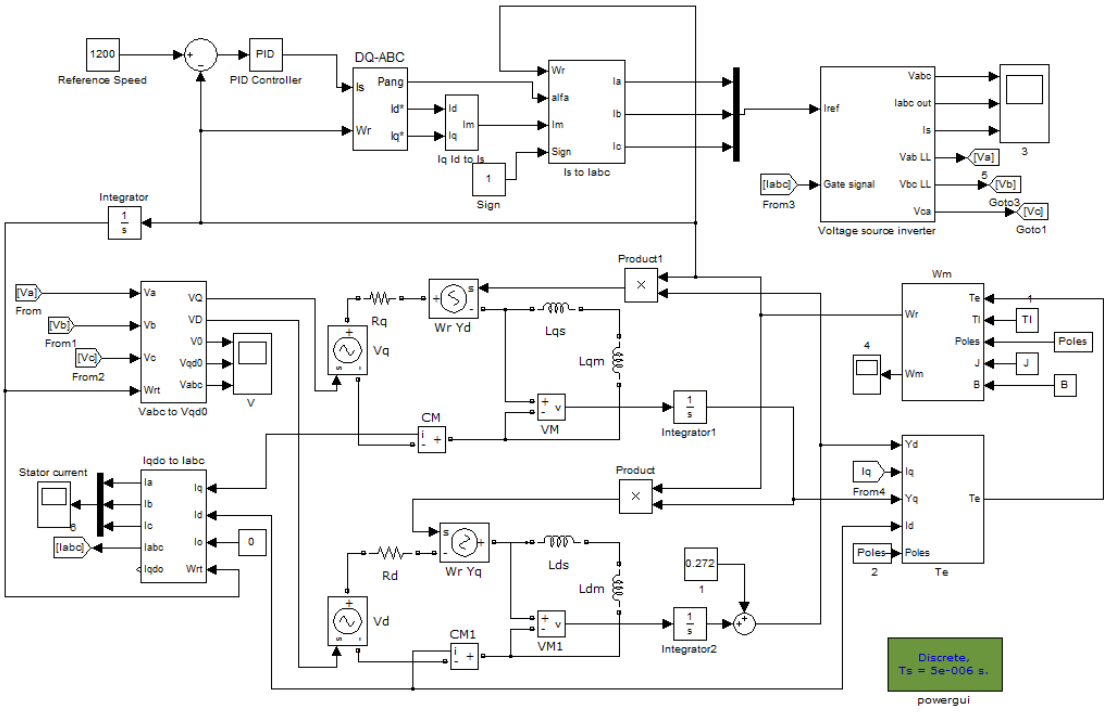

Figure 3-10: PMSM Model Implemented in Simulink

3.3 Diesel Engine Generator System Dynamics

Since the engine and generator are rigidly coupled together in a SHEV configuration, to

evaluate the overall energy efficiency, the engine generator can be viewed as one single unit. The efficiency of the unit is the product of efficiencies of the engine and the generator. The block diagram of simplified engine torque production model and engine dynamics are shown in Figure 3-11.

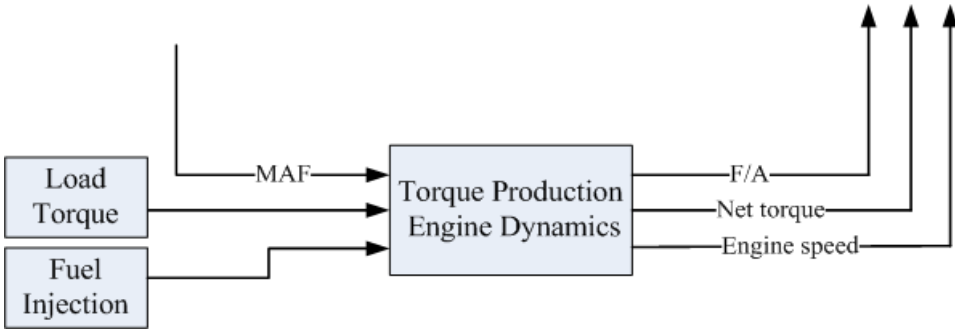

Figure 3-11: Torque Production and Engine Dynamics Sub-model

To analyze the overall system dynamics, the engine model can be simplified to a torque production model. The general equation of the engine model can be summarized as

$$T = f(\omega, \dot{m}_{ff}) \qquad \textbf{3-20}$$

where, T is the torque of the engine. It is a function of the n (engine speed in rad/s) and fuel flow rate $\dot{m}_{ff}$ (g/s). For the generator set application in a SHEV, engine speed control is the main concern; hence the model can be simplified to only include the average torque production sub-model [33].

Average indicated torque production of a diesel engine:

$$T_{eng} = 2\pi\eta Q_{LHV}\dot{m}_{ff} \qquad \textbf{3-21}$$

Engine power

$$P_{net} = P_{ind} - P_{loss} - P_{load} \qquad \textbf{3-22}$$

For a steady state operation

$$P_{ind} = P_{loss} + P_{load} \quad \textbf{3-23}$$

$$P_{load} = P_{gen} \quad \textbf{3-24}$$

For generator set electrical torque is expressed as

$$T_{gen} = \frac{3}{2} P \lambda_m i_q \quad \textbf{3-25}$$

The combined system dynamics of the engine generator set is obtained by applying torque balance to the system:

$$2\pi\eta Q_{LHV} \dot{m}_{ff} - T_g - B\omega = J \frac{d\omega}{dt} \quad \textbf{3-26}$$

This model determines the system speed by calculating the torque produces from the combustion of the fuel and deducts the load torque. The engine is controlled through the injection and the generator is considered a resistance torque to the engine. Assuming the shaft connecting the generator and the engine crankshaft is rigid, J is the rotational inertia and B is the damping coefficient of the engine-generator set. This quasi-static engine model is suitable and sufficient for system level control studies assuming the engine transients are much faster than the system level energy dynamics.

3.4 NOx and Soot Emission Model

NOx and Soot are the major emissions produced by diesel engines. To meet the stringent emission legislations, a large amount of effort was spent by engine manufacturers and researchers on engine combustion. Engine tests and emission models can be used to measure and predict engine out emissions. Engine tests are expensive and time consuming, so it will be beneficial to use emission models to carry out a preliminary

calibration of the engine, and then validate/fine tune it during the actual testing phase. Most of the widely used emission models are based on steady state engine maps which are not able to handle different engine conditions other than the tested condition and are overwhelmed by the excessive numbers of parameters [35, 36 and 37].

A model based NOx and soot emission estimation with the impact of EGR has been presented. This estimation consists of three parts: a combustion, NOx and soot prediction model. The combustion thermodynamic sub-model is based on a single-zone, double Wiebe function. It uses fuel injection rate, injection timing and intake boost to calculate the dynamic parameters such as heat release rate and the mean combustion temperature that are to be used by the emission sub-model for predicting emissions. EGR can reduce NOx emissions; however, a high rate of EGR can result in a high level of soot emission; in order to show this trade off quantitatively, EGR has been included in the combustion model. The correlation between the EGR ratio and exhaust products molar concentration has been simulated based on combustion temperature and chemical kinetics. NOx and soot estimation are modeled, based on the extended Zeldovich mechanism and Hiroyasu's two-step empirical model, respectively. The rate coefficients for principal reactions which govern the formation of thermal NOx have been evaluated with empirical test data.

3.4.1 Diesel Combustion Model

The performance of the NOx and soot model is directly related to the quality of the combustion model. In order to predict engine emissions, the combustion process should

be estimated first. The combustion thermodynamic sub-model is based on a single-zone, double-Wiebe function [38]. It uses fuel injection to provide the necessary parameters such as heat release rate and the mean combustion temperature to be used by the emission sub-model for predicting emissions are shown in Figure 3-12.

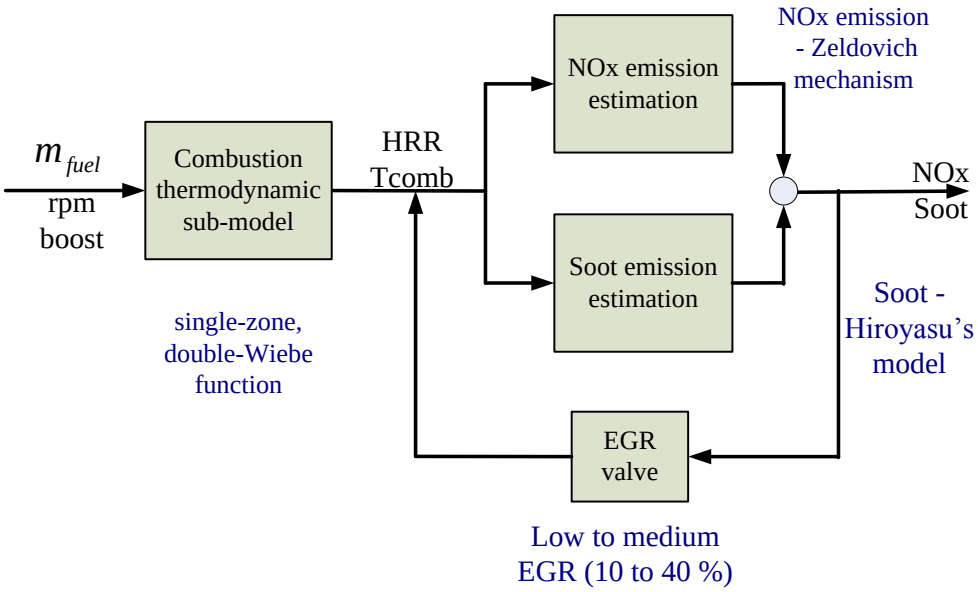

Figure 3-12: Block Diagram of the Model Based NOx and Soot Estimation with EGR Effect

The governing equation of combustion thermodynamic is shown in 3-27.

$$x_b = (1-\alpha_{wall})\left\{1-\exp(-a\left(\frac{\theta-\theta_0}{\Delta\theta}\right)^{m+1}\right\}+\alpha_{wall}\left\{1-\exp(-a\left(\frac{\theta-\theta_0}{K_{wall}\Delta\theta}\right)^{m+1}\right\} \quad \textbf{3-27}$$

where x_b is the mass fraction burned, θ is the crank angle, θ_0, is the crank angle at the start of combustion, a and $\Delta\theta$ are adjustable constants that determine the combustion duration, and m is an adjustable parameter that fixes the shape of the combustion progress curve. α_{wall} is the fraction of the mixture that burns in the slow combustion

region and K_{wall} is the ratio of the slow burn duration to the standard burn duration.

Apparent Heat Release Model

Combustion characteristics are described by heat release rate. EGR can alter heat release magnitude and phasing, delay ignition and prolong combustion duration. It is critical to capture the combustion characteristics with influences of EGR for emission evaluations [38]. The heat release model is based on the first law of thermodynamics for an open system. Assuming the cylinder charge is a single zone and using the ideal gas law, the heat release during combustion, dQ_{ch} on a crank angle basis is given by [39]:

$$\frac{dQ_{app}}{d\theta} = \frac{dQ_{ch}}{d\theta} - \frac{dQ_{ht}}{d\theta} = \frac{1}{\gamma - 1}\left[\gamma p \frac{dV}{d\theta} + v\frac{dp}{d\theta}\right] \qquad \textbf{3-28}$$

$\gamma = cp/cv$ is the ratio of the specific heats, dQ_{ht} is the charge-to-wall heat transfer

By subtracting the heat transfer from the chemical heat release and neglecting the crevice volume, blow-by and the fuel injection effects, we arrived at an apparent heat release equation. Apparent heat release values are very often preferred over gross heat release values because it reduces the amount of computation and avoids the need for heat transfer parameters to be specified.

3.4.2 EGR Model

Most of diesel exhaust consists of the compound NO, but once it is in the presence of oxygen it tends to oxidize and produce NO_2. The production of NOx depends on the

amount of oxygen available and temperature. As cylinder gas temperatures reach above 1800 K, the rate of which NOx production increases vastly. To reduce NOx from the diesel combustion, the combustion temperature should be lowered or reduce the oxygen availability in the cylinder. EGR is effective in lowering both the combustion temperature and availability of oxygen. Figure 3-13 shows the typical implementation of EGR [19].

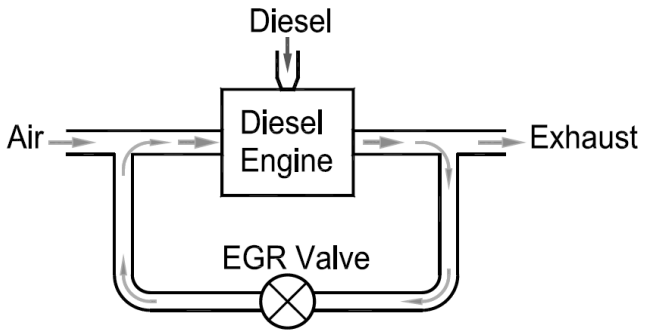

Figure 3-13: EGR Configuration [19]

Carbon dioxide (CO_2), an exhaust compound is used to calculate the amount of EGR. By knowing the concentration of CO_2 of both the intake and exhaust, the amount of EGR introduced into the cylinder can be calculated by Equation 3-29 [19].

$$EGR\ ratio = \frac{\text{intake } CO_2 \text{ concentration}}{\text{exhaust } CO_2 \text{ concentration}} \qquad \textbf{3-29}$$

As CO_2 enters the cylinder, it increases the heat capacity of the air charge, which in turn lowers the specific heat capacity ratio, and as a result, lowers the flame temperature. At the same time, EGR reduces the availability of oxygen since the fresh charge is being replaced by the exhaust gas from the previous cycles. By limiting the availability of oxygen, the fuel has more time to mix due to the longer ignition delay. As ignition delay increases, keeping fueling events constant, combustion occurs at a later stage of the

expansion stroke [40]. This causes a lower peak cylinder pressure, which yields a lower cylinder temperature, thus achieving lower NOx emissions. Equation 3-30 shows the governing reaction for complete combustion with EGR effects.

$$\mathrm{C}_{\alpha}H_{\beta} + a(O_2 + 3.76N_2) + \left(\frac{\alpha \times EGR}{1-EGR}\right)CO_2 + \left(\frac{\frac{\beta}{2}EGR}{1-EGR}\right)H_2O + \frac{\left[a-(\alpha+\frac{\beta}{4})\right]EGR}{1-EGR}O_2$$

$$+3.76 \times a \times \frac{EGR}{1-EGR}N_2 \rightarrow \left(\frac{\alpha}{1-EGR}\right)CO_2 + \left(\frac{\beta}{2(1-EGR)}\right)H_2O + \frac{a-(\alpha+\frac{\beta}{4})}{1-EGR}O_2 + \frac{3.76 \times a}{1-EGR}N_2 \quad \textbf{3-30}$$

Assuming ambient air has the concentration of 21% O_2, 78% N_2 and 1% H_2O by mass. The initial concentrations of the intake species can be defined as the following values:

$$N_{O_2}(1) = M_{air\_fresh} \times 21\% / M_{EGR} \times n \quad \textbf{3-31}$$

$$N_{N_2}(1) = M_{air\_fresh} \times 78\% / M_{EGR} \times n \quad \textbf{3-32}$$

$$N_{H_2O}(1) = 1\% / 100 \times n \quad \textbf{3-33}$$

$$N_{CO_2}(1) = EGR / (1-EGR) / N_{total} \times n \quad \textbf{3-34}$$

A complete combustion cycle is 720 crank angles. A combustion cycle can be also defined as 7200 computational steps with a 0.1 crank angle degree resolution. According to the complete combustion equation with EGR, the concentrations of species of the current step are the sum of the previous step value plus the new reaction formation in the current step, as shown in the following equations:

$$N_{O_2}(i) = N_{O_2}(i-1) + N_{rec-O_2} \quad \textbf{3-35}$$

$$N_{CO_2}(i) = N_{CO_2}(i-1) + N_{rec-CO_2} \quad \textbf{3-36}$$

$$N_{H_2O}(i) = N_{H_2O}(i-1) + N_{rec-H_2O} \quad \textbf{3-37}$$

where instantaneous rate of species are given by

$$N_{rac\_O_2} = -HRR(i) \times stepsize / Q_{LHV} / 13.7 \times (1 + \beta / 4) \quad \textbf{3-38}$$

$$N_{rac\_CO_2} = HRR(i) \times stepsize / Q_{LHV} / 13.7 \times (\lambda / (1 - EGR)) \quad \textbf{3-39}$$

$$N_{rac\_H_2O} = HRR(i) \times stepsize / Q_{LHV} / 13.7 / (\beta / 2 / (1 - EGR)) \quad \textbf{3-40}$$

α=1, β=1.8, Q_{LHV}=42.9 MJ/kg

The total instantaneous molar mass of all the products is given by:

$$N_{total}(i) = N_{H_2O}(i) + N_{CO_2}(i) + N_{O_2}(i) + N_{N_2}(i) \quad \textbf{3-41}$$

The total molar number of product substances is the sum of the molar number of each product. They are H_2O, CO_2, O_2, and N_2.

$$[O_2] = N_{O_2}(i) / N_{\text{instantaneous}}(i) \quad \textbf{3-42}$$

$$[CO_2] = N_{CO_2}(i) / N_{\text{instantaneous}}(i) \quad \textbf{3-43}$$

$$[H_2O] = N_{H_2O}(i) / N_{\text{instantaneous}}(i) \quad \textbf{3-44}$$

The instantaneous molar fraction of a species is expressed by the above equations. where: $[O_2]$, $[CO_2]$, $[H_2O]$ are the molar fraction of the corresponding species, M_{EGR} is mass of the intake in kg, M_{air_fresh} is the sass of the intake fresh air in kg, n is the number of moles of intake; HRR is Heat Release Rate of the combustion per step size.

It has been well known that, at the moderate EGR rate, it is the almost 'free NOx reduction' region where the application of low-to-moderate EGR results in NOx reduction without the associated soot penalty and sacrifice noticeable engine efficiency.

As EGR is progressively increased, the increased heat capacity of the recycled inert gases, together with the reduced oxygen concentration results in reduced local flame temperatures during the combustion process and thus, a reduced rate of NOx formation.

However, the soot emissions tend to increase rapidly as EGR is increased (Slope 1-classical NOx-soot trade-off). Soot emissions from diesel engines are the result of the difference between the soot production and soot oxidation processes [41]. The lowered combustion temperature and the charge dilution are thought to reduce the soot oxidation rates associated with the low flame temperatures of diluted mixtures, thereby increasing the soot emissions. Due to the above mentioned reasons, low to medium levels of EGR has been simulated in this study and been performed in the diesel engine emission control. Various engine loads and operating conditions are tested to show the impact of EGR on NOx and soot emissions. The estimation results are validated with empirical tests on a state-of-the-art common rail direct injection diesel engine.

3.4.3 NOx Emission Model

The extended Zeldovich mechanism developed in the past is still adequate to provide satisfactory prediction of NOx emissions [42, 43]. Its mechanism can be decoupled from the main combustion process, based on consideration of the equilibrium values of temperature, stable species, O atoms, and OH radicals.

The three reactions included in the Zeldovich mechanism are [43]:

$$O + N_2 \underset{k_r}{\overset{k_f}{\rightleftharpoons}} N + NO \qquad \textbf{3-45}$$

$$N + O_2 \underset{k_r}{\overset{k_f}{\rightleftharpoons}} O + NO \qquad \textbf{3-46}$$

$$N + OH \underset{k_r}{\overset{k_f}{\rightleftharpoons}} H + NO \qquad \textbf{3-47}$$

First two reactions simulate the thermal NOx formed in the post-combustion combined with the third equation, well-known extended Zeldovich mechanism is given. A third reaction has been shown to contribute to the formation of thermal NOx, particularly at near-stoichiometric conditions and in fuel-rich mixtures.

NO net formation rate based on the extended Zeldovich mechanism is given by:

$$\frac{d[NO]}{dt} = k_{f1}[O][N_2] + k_{f2}[N][O_2] + k_{f3}[N][OH] - k_{r1}[NO][N] - k_{r2}[NO][O] - k_{r3}[NO][H] \qquad \textbf{3-48}$$

All concentrations have units of gmol/m^3, where k_{f1}, k_{f2}, k_{f3} are the rate constants for the forward reaction respectively, and k_{r1}, k_{r2}, k_{r3} are the corresponding reverse rate constants. The concentrations of O, H, and OH are required to calculate the formation rates of NO and N.

For a diesel combustion, CO_2, CO, H_2O, H_2, O_2, N_2, H, O, NO and OH are the typical combustion products. Once the chemical equilibrium has been reached, the concentrations of species can be defined as [11, 12]:

$$k_{f1}[O][N_2] = k_{r1}[O][N_2] \qquad \textbf{3-49}$$

$$k_{f2}[N][O_2] = k_{r2}[NO][O] \quad \textbf{3-50}$$

$$k_{f3}[N][OH] = k_{r3}[NO][H] \quad \textbf{3-51}$$

The equilibrium concentration of N, O, and OH can be estimated from the combustion model with the EGR effect blended in.

3.4.4 Soot Emission Model

Many soot models are based on the understanding of the mechanisms and phenomenology of soot formation. Soot emission estimation is a challenging task because of the complicated chemical mechanism and particle dynamics. In this study the popular soot model proposed by Hiroyasu et al. [44] is applied to the estimation of soot emissions. This model employs two Arrhenius expressions for the rates of soot formation and oxidation. Although the Hiroyasu model did not provide detailed information about the formation of soot, it could still effectively predict soot emission [3]. The required parameters such as combustion temperature and oxygen pressure that are used in this model are estimated in the previous combustion model with the EGR effect

Hiroyasu's two-step empirical soot model involves two reactions steps: the formation step where: soot is directly related to fuel vapor molecules, and the oxidation step where soot particles decrease by the attack of molecular oxygen.

$$\frac{dm_{soot}}{dt} = \left(\frac{dm_{soot}}{dt}\right)_{form} - \left(\frac{dm_{soot}}{dt}\right)_{oxid} \quad \textbf{3-52}$$

$$\frac{dm_{soot\_form}}{dt} = A_1 \exp\left(-\frac{T_{A1}}{T}\right) m_{fuelv} \left(\frac{P_{gas}}{P_{gas\_ref}}\right)^{n1} \quad \textbf{3-53}$$

$$\frac{dm_{soot\_oxid}}{dt} = A_2 \exp(-\frac{T_{A2}}{T}) m_{soot}^{n2} (\frac{P_{O_2}}{P_{O_2\_ref}})^{n3} \quad \textbf{3-54}$$

where A_1 is the constant for soot formation, A_2 is the constant for soot oxidation, T_{A1} and T_{A2} are activation temperature and P_{gas} and P_{gas_ref} are gas pressure and reference gas pressure.The follow values are used: $A_1=1.2x10^{-4}$, $A_2=3800$, $T_{A1}=6313$, $T_{A2}=7070$, $n_1=2.4$, $n_2=1$, $n_3=1$, $P_{gas\_ref}=0.1$ and $P_{O2\text{-}ref}=0.021$.

Table 3-3: Single Cylinder Research Engine Specifications

Single Cylinder Research Engine Specifications	
Cylinders	1
Type	4-Stroke
Displacement	0.78 Liters
Bore	96 mm
Stroke	107.8 mm
Compression Ratio	15.5:1
Injection System	Common Rail

3.4.5 Engine Test Platform

A modern single cylinder research engine coupled to a DC dynamometer was used to provide empirical tests result to tune the emission models. The engine specifications are given in Table 3-3 and the overall system setup is shown in Figure 3-14.

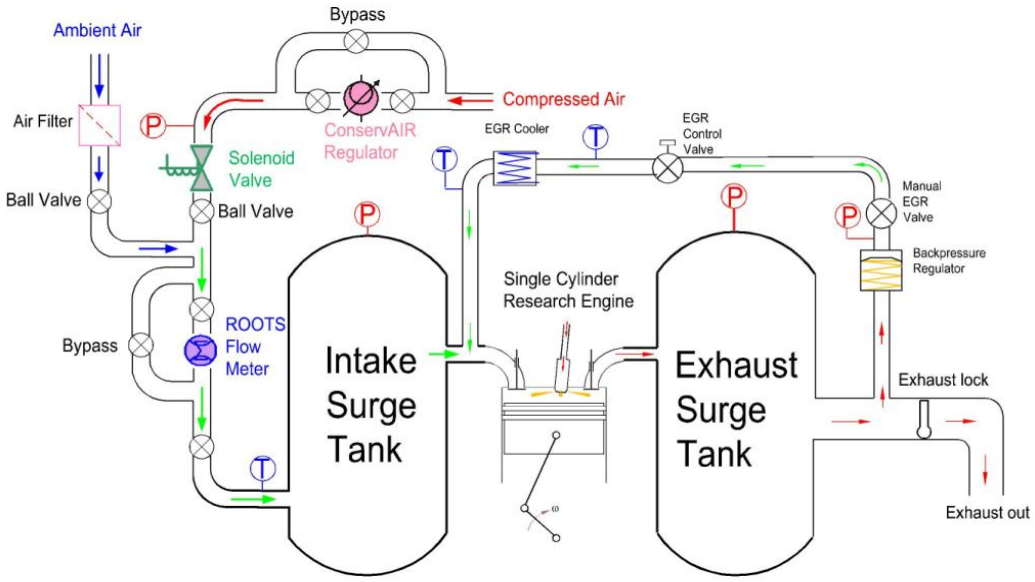

Figure 3-14: Single Cylinder Research Engine Test Platform

Clean and dry combustion air was provided from an oil-free compressor and the intake pressure was precisely controlled by electro-pneumatic pressure regulators. The exhaust backpressure was controlled through a pneumatically-actuated flow-control valve and an electro-pneumatic pressure regulator. This allowed independent control of the boost and exhaust backpressures. The EGR was cooled with the engine coolant and the EGR amount was controlled with a combination of the EGR valve position and exhaust backpressure control. In-house LabVIEW codes were developed to establish CAN

communication to the EGR valve and for data acquisition. The engine coolant and lubricating oil conditions were monitored and controlled at a fixed temperature of 80℃ to minimize discrepancies in the test results.

A dual-bank exhaust analyzer system (NOx, HC, CO, CO_2, O_2) has been instrumented for the tests; normally one for the exhaust emissions and the other for the intake gas concentrations. NOx was measured with a CAI 6000 Series chemiluminescence detector. An AVL smoke meter was used to measure soot indicated by the Filter Smoke Number (FSN). In order to compare measurements with prediction values, the relation between FSN and smoke mass concentration in [mg/m3] is used which given in Equation 3-55 [45],

$$Smoke(mg/m^3) = \frac{1}{0.405} \cdot 5.32 \cdot FSN \exp(0.3062 \cdot FSN) \qquad \textbf{3-55}$$

3.5 Model Predictive Control of the Diesel Engine Generator Set

The diesel engine is controlled by an electric governor with a DC actuator to rotate a PMSM. A three-phase PWM converter, inverter, and a PWM dc–dc converter are usually included in the system to create a DC bus; the voltage of the DC will be kept constant to charge the battery pack. The required power output from the engine generator set P_{out} can be defined by the driver's gas pedal signal. The driver's pedal signal is in the range of 0 to 100%, it is divided into 8 different segments corresponding to each of the engine operating points that developed in the previous chapter. Higher driver gas pedal signal

level represents more power demand from the engine generator set to charge and maintain the battery SOC. The power output of the engine generator set is dependent on the engine speed. The reference to engine speed is referred to the high order approximation of power-speed relationship that is obtained from the experimental mapping. The engine speed is regulated by an actuator that controls the fuelling to the engine. To control the power output and improve the dynamic response of the engine generator set, MPC is applied to provide predictive features to close control the engine speed.

3.5.1 Basics of Model Predictive Control

The MPC is applied to manage the power of the engine generator set in this study. MPC is a control method that uses an explicit process model to predict future behaviour of a system. An optimal input is computed by solving an open-loop optimal control problem over a finite number of future samples. A cost function is minimized at each sampling time to obtain optimal control inputs for a system. The solution to the optimization problem is a vector of input signals to the system that minimizes a chosen performance criterion without violating any of the constraints of the system. An advantage of MPC is that constraints can be accounted for when the input signal is computed [46, 47]. A general structure diagram of MPC is illustrated in Figure 3-15.

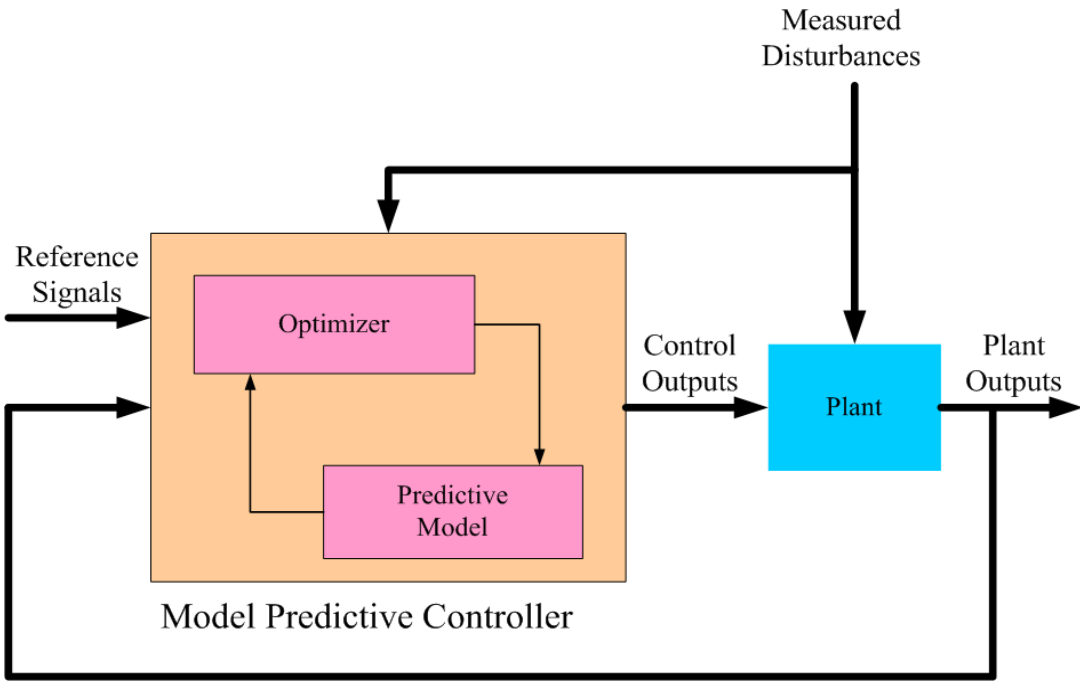

Figure 3-15: MPC Diagram

In order for the controller to predict the future system behaviour, system model has to be defined first. Then the system model needs to be time discretized for MPC to use. Inside the MPC, it consist an optimizer and a predictive model. Based on the predicted model output and current system output, the error is calculated. The errors are fed to the optimizer. The future optimal control sequence is calculated in the optimizer based on the objective function and system constraints. Once the optimal input sequence has been computed, only the first sample is applied to the plant, according to the receding horizon policy. The starting point of the optimal control scheme is periodically updated through feedback and the prediction horizon accordingly shifted in time, so that the control scheme sees a predicted behaviour which is naturally updated to account for the measured changes of the system.

3.5.2 Control Oriented Diesel Engine Generator Set Model

A dynamic model of the engine generator set is derived from a first principles analysis of the system dynamics. This model is the basis for the MPC algorithm, the dynamic PMSM model in the d-q rotor frame can described as follows:

$$\frac{di_d}{dt} = \frac{1}{L}\left(u_d - Ri_d - P\omega_r L i_q\right) \quad \textbf{3-56}$$

$$\frac{di_q}{dt} = \frac{1}{L}\left(u_q - Ri_q - P\omega_r (Li_d + \lambda_m)\right) \quad \textbf{3-57}$$

$$\frac{d\omega_r}{dt} = \frac{1}{J}(T_{eng} - T_{gen} - B\omega_r) \quad \textbf{3-58}$$

Where

$$T_{eng} = 2\pi\eta Q_{LHV}\dot{m}_{ff} \quad \textbf{3-59}$$

$$T_{gen} = \frac{3}{2}P(\lambda_d i_q - \lambda_q i_d) \quad \textbf{3-60}$$

3-57 and 3-58 defines the current dynamics of d-axis and q-axis in the PMSM, furthermore, 3-59 relates the torque between the engine and the generator and accounts for inertia, damping of the system. where R is the stator resistance, i_d is the d-axis current, i_q is the q-axis current, U_d is the d-axis stator voltage, U_q is the q-axis stator voltage, L is the stator inductance, stator inductance in d and q axis are assumed to be equal (i.e Ld=Lq), P is the number of pole pairs, ω_r is the system rotational speed in rad/s, λ_m is the flux linkage by the permanent magnets, J is the system moment of inertia, B is the damping coefficient, T_{eng} is the engine torque generated by the diesel engine, the

engine combustion processes have been neglected, the engine is treated as a torque source to reduce the model complexity, the engine torque is related with thermal efficiency, lower heating value of the fuel and the fuel flow rate. T_{gen} is the generator load torque.

The above dynamic model of PMSM consists nonlinear equations. It needs to be linearized and discretized so that can be used within the MPC algorithm. EGR control for emission was not implemented in this MPC design.

3.5.3 Model Linearization

In controlling the PMSM, for model simplicity purpose, a common technique is to align the magnet flux linkage to d-axis and keep stator current vector to q-axis direction [48]. As a result, i_d is zero. For a PMSM used in generator application, the permanent magnet flux is constant, so that electromagnetic torque is linearly proportional to q-axis current. Therefore, the electromagnetic torque can be expressed in a linear form as following

$$T_{gen} = \frac{3P\lambda_m}{2} i_q = k_t i_q \qquad \textbf{3-61}$$

$$k_t = \frac{3P\lambda m}{2} \qquad \textbf{3-62}$$

Where, k_t is motor torque constant.

Combining 3-58, 3-59 and 3-61, one arrives at the state space representation expressed in 3-63, note that $\dot{m}_{ff}$ is the fuel flow rate to the engine, not a state space variable.

$$\dot{x} = \begin{bmatrix} -\frac{R}{L} & -\frac{P\lambda_m}{L} \\ -\frac{k_t}{J} & -\frac{B}{J} \end{bmatrix} \begin{bmatrix} i_q \\ \omega_r \end{bmatrix} + \begin{bmatrix} \frac{1}{L} & 0 \\ 0 & \frac{2\pi\eta Q_{LHV}}{J} \end{bmatrix} \begin{bmatrix} u_q \\ \dot{m}_{ff} \end{bmatrix} \qquad \textbf{3-63}$$

The linearised state space model of PMSM can be written standard form as:

$$\dot{x} = Ax + Bu$$
$$y = Cx + Du$$

Thus, the system matrices are given by 3-64 to 3-68

$$x = \begin{bmatrix} i_q \\ \omega_r \end{bmatrix} \quad \textbf{3-64}$$

$$u = \begin{bmatrix} u_q \\ \dot{m}_{ff} \end{bmatrix} \quad \textbf{3-65}$$

$$A = \begin{bmatrix} -\frac{R}{L} & -\frac{P\lambda_m}{L} \\ -\frac{k_t}{J} & -\frac{B}{J} \end{bmatrix} \quad \textbf{3-66}$$

$$B = \begin{bmatrix} \frac{1}{L} & 0 \\ 0 & \frac{2\pi\eta Q_{LHV}}{J} \end{bmatrix} \quad \textbf{3-67}$$

$$C = \begin{bmatrix} 1 & 0 \\ 0 & 1 \end{bmatrix} \quad \textbf{3-68}$$

The specifications for the engine-generator set used in this study are listed in Table 3-4:

Table 3-4: Specifications for the Engine-Generator Set

Stator resistance	2.15ohm
Stator inductances	0.79 mH
Magnetic Flux	0.42 Wb
Inertia	0.03 kgm^2
Damping coefficient	0.05 Nms/rad
Number of pole pair	1

3.5.4 Time Discretization

Since MPC controller has to deal with both current and future system dynamics, MPC requires a discrete time model. In order to capture a correct approximation of the fastest dynamics, the time step has to be small enough with respect to capture fast changing system behaviours. However, the main drawback of a very small time step is that the coefficients that describe the slow dynamics associated to the speed are extremely close to zero, with numerical problems [49]. Moreover, very small control cycles may cause a computational overflow of a computer processor. The previously presented continuous time state space equation is rewritten to the discretized one by using zero order hold method [50] at sampling time Ts=1 ms, system matrices 3-66 and 3-67 were computed using the system specification values and at the following operating point: ω_r=167.5 rad/s, m_f=0.508 g/s and u_q=190 V.

The resulting discrete time model that obtained with zero-hold discretization method is given as:

$$A=\begin{bmatrix} 0.06691 & -0.1826 \\ -0.007212 & 1.001 \end{bmatrix} \quad \textbf{3-69}$$

$$B=\begin{bmatrix} 0.4352 & -0.3689 \\ -0.006415 & 2.876 \end{bmatrix} \quad \textbf{3-70}$$

$$C=\begin{bmatrix} 1 & 0 \\ 0 & 1 \end{bmatrix} \quad \textbf{3-71}$$

3.5.5 Cost Function and Control Law Parameters

The speed controller is used to regulate the speed of the engine generator set to the desired value. The speed controller adjusts the fuel quantity delivered to the combustion

chamber according to the magnitude of the speed error. The speed error is the difference between the actual speed and desired reference.

The problem can be formulated as follows

$$\dot{x} = f(x(t), u(t)) \qquad \textbf{3-72}$$

$$x(0) = x_0 \qquad \textbf{3-73}$$

where $x(t) \in R_x^n$ is the state vector and $u(t) \in R_u^n$ is the input vector of the model.

The predicted state sequence generated by the linear state-space model with input u(t) can be expressed as

$$x(k \mid k) = x(k) \qquad \textbf{3-74}$$

$$x(k+1 \mid k) = Ax(k) + Bu(k \mid k)$$

$$x(k+2 \mid k) = A^2 x(k) + ABu(k \mid k) + Bu(k+1 \mid k)$$

$$\vdots$$

The output of the model can be described as:

$$y = g(x(t), u(t)) \qquad \textbf{3-75}$$

where $y \in R_y^n$ is the output vector.

Based on a nonlinear mean value engine model, linearization was done at multiple operating points, then a linear MPC strategy was implemented. The developed MPC controller controls and minimizes the error between the requested engine speed and the actual engine speed, by tracking and manipulating fuel injection to perform power control. MPC solves an optimal control problem in each discrete-time step based on the previous time step over prediction horizon. Optimization is the procedure to find the best

alternative for objective/objectives. Enable to do optimization; a quantitative measure of performance of the system is required. Then optimization task is to find a parameter that maximizes/minimizes the objective equation. The optimization equation formulates the state variable and the corresponding control input u(t) for $t \in [0,k]$ should be chosen in order to track speed reference so that the engine speed error can be minimized.

The objective function $J \in R$ is chosen to be quadratic and including the input and output variables. The model predictive control action at time k is obtained by solving the optimization problem [51, 52]:

$$\min J(k) = \sum_{j=1}^{N_p} \left| Q[Y(k+i|k) - R(k+i)] \right|^2 + \sum_{j=1}^{N_u} \left| P[U(k+i)] \right|^2 \qquad \textbf{3-76}$$

subject to

$$x^0 = x(t_0) \qquad \textbf{3-77}$$

$$U_{\min} \le u^k \le U_{\max} \qquad \textbf{3-78}$$

$$\Delta U_{\min} \le \Delta u^k \le \Delta U_{\max} \qquad \textbf{3-79}$$

where

i=0, …,N_p -1

$$Q = diag\left\{\Gamma_1^u, \cdots, \Gamma_{N_u}^u\right\} \qquad \textbf{3-80}$$

and

$$P = diag\left\{\Gamma_1^u, \cdots, \Gamma_{N_2}^u\right\} \qquad \textbf{3-81}$$

are the weighting on the control deviation and the weighting on the rate of change of the difference control action. The value of weighting Q and P are given as follows,

$$Q=\begin{bmatrix}1 & 0\\ 0 & 1\end{bmatrix} \qquad \textbf{3-82}$$

$$P=\begin{bmatrix}0.05 & 0\\ 0 & 0.05\end{bmatrix} \qquad \textbf{3-83}$$

By giving P a heavier weight than Q, the reference velocity should be closely followed is considered to be more important than using only a little supplied voltage and a small quantity in the fuel injection to the engine. When appropriate weights are chosen, system reaches the desired velocity quick and trying to hold it.

The first term in 3-76 represents the future output error and the second term is a penalty term for the manipulated variable that moving away from its objective. Assuming that estimates of $x(k)$ is available at time k. The number of samples one looks ahead is called the prediction horizon N_p. The control horizon N_u is the number of samples that the optimal input is calculated for. r(k) is the current sample of the output reference. "(k+i|k)" denotes the value predicted for time k+i. This predictive value is based on the information available at time k. The predicted output Y respect to the reference R and the control action U will be minimized.

Model parameter weightings and estimator gain were tuned to ensure MPC control response speed and minimize overshoot. The control horizon should be kept short to ease the computational effort, however an excessive short N_u can cause short-sighted control can resulting a cautious control action. On the other hand, making prediction horizon N_p short will tend to lead to an aggressive control action. Generally, it is desire to choose a

large prediction horizon to complete capture the consequences of the control actions. Prediction horizon and control horizon are given with value of 5 and 1 respectively in this study.

The p step ahead prediction becomes:

$$R(k+1)=\begin{bmatrix} r(k+1) \\ r(k+1) \\ \vdots \\ r(k+p) \end{bmatrix} \qquad \textbf{3-84}$$

are the vector of the reference trajectories.

The constraints imposed on the control signals and state variables are listed as follows. The constraints on the states are chosen as to guarantee signals stay at physically reasonable values.

$$u_{\min}=0\le\begin{bmatrix} u_q \\ m_f \end{bmatrix}\le u_{\max}=\begin{bmatrix} 350 \\ 2.5 \end{bmatrix} \qquad \textbf{3-85}$$

$$\frac{du_{\min}}{dt}=\begin{bmatrix} -0.3 \\ -0.015 \end{bmatrix}\le\begin{bmatrix} \frac{du_q}{dt} \\ \frac{dm_f}{dt} \end{bmatrix}\le u_{\max}=\begin{bmatrix} 0.3 \\ 0.015 \end{bmatrix} \qquad \textbf{3-86}$$

$$x_{\min}=0\le\begin{bmatrix} i_q \\ n_r \end{bmatrix}\le x_{\max}=\begin{bmatrix} 50 \\ 364 \end{bmatrix} \qquad \textbf{3-87}$$

where U_{max} is the upper bound of the control input vector and U_{min} is the lower bound of the control input vector. dU_{max}/dt and dU_{min}/dt are bounds of the change rate for input vector.

A MPC controller use quadratic programming (QP) to solve the objective equation of the control problem [53]. The QP is solved by **quadprog** function in MATLAB. The optimisation problem 3-76 can be rewritten in a standard QP form in 3-89,

$$\min\left(\frac{1}{2}x^T Hx + c^T x + \alpha\right) \quad \textbf{3-88}$$

subject to

$Ax \leq b;$

$x \leq u;$

The goal of the QP is to determine the x for which the function is minimum. H is a symmetric matrix called the Hessian matrix, c is a vector of constants and α is the scalar constant.

For a system with two outputs y_1 and y_2 as the developed diesel engine generator model, therefore 3-77 can be rewritten as [54]

$$\min J = \left\{\Gamma_1^2[y_1(k+i\,|\,k) - r_1(k+i)]^2 + \Gamma_2^2[y_2(k+i\,|\,k) - r_2(k+i)]^2\right\} + \left\{\Gamma_1^2[u_1(k+i\,|\,k)]^2 + \Gamma_2^2[u_2(k+i\,|\,k)]^2\right\} \quad \textbf{3-89}$$

$$Y = \begin{bmatrix} y_1 & y_2 \end{bmatrix}^T \quad \textbf{3-90}$$

$$U = \begin{bmatrix} u_1 & u_2 \end{bmatrix}^T \quad \textbf{3-91}$$

$$R = \begin{bmatrix} r_1 & r_2 \end{bmatrix}^T \quad \textbf{3-92}$$

R is the reference matrix.

The system output change for a unit input change is given by step response model, defined as $\{0, s_1, s_2, \ldots, s_n\}$ [54, 55]. If we assume the system settles after n steps, the system model can be defined as

$$y(k) = \sum_{i=1}^{n} s_i \Delta u(k-i) + s_n u(k-n-1) \quad \textbf{3-93}$$

Equation 3-93 allows us to compute the system output for any input sequence. Since the system matrix has a size of 2x2, therefore, the system can be model by the following four transfer functions.

For operating point #3, the system matrix was identified as 3-69 to 3-71, the corresponding model of the first output to the first input can be modeled by the following transfer function,

$$\frac{y_1}{u_1} = \frac{i_q}{u_q} = \frac{1266z + 2152}{z^2 + 2723.2z - 6537} \qquad \textbf{3-94}$$

The corresponding transfer function of the first output to second input can be modeled as 3-95,

$$\frac{y_1}{u_2} = \frac{i_q}{m_f} = \frac{-2658.2}{z^2 + 2723.2z - 6537} \qquad \textbf{3-95}$$

The corresponding transfer function of the second output to first input can be modeled as 3-96,

$$\frac{y_2}{u_1} = \frac{n}{u_q} = \frac{-1.5285e6}{z^2 + 2723.2z - 6537} \qquad \textbf{3-96}$$

Lastly, the corresponding transfer function of the second output to second input can be modeled as 3-97,

$$\frac{y_2}{u_2} = \frac{n}{m_f} = \frac{2.9e3z + 7.8249e6}{z^2 + 2723.2z - 6537} \qquad \textbf{3-97}$$

The prediction horizon of MPC is 5, the step response coefficients for all the transfer function are,

$$s_1 = \begin{Bmatrix} 0 \\ 0.4830 \\ 0.5028 \\ 0.5229 \\ 0.5436 \end{Bmatrix} \quad \textbf{3-98}$$

$$s_2 = \begin{Bmatrix} 0 \\ -0.0950 \\ -0.1961 \\ -0.2995 \\ -0.4055 \end{Bmatrix} \quad \textbf{3-99}$$

$$s_3 = \begin{Bmatrix} 0 \\ -5.4652 \\ -11.273 \\ -17.223 \\ -23.316 \end{Bmatrix} \quad \textbf{3-100}$$

$$s_4 = \begin{Bmatrix} 0 \\ 29.066 \\ 58.828 \\ 89.312 \\ 120.536 \end{Bmatrix} \quad \textbf{3-101}$$

By substituting system response coefficients and input into equation 3-93, the system output can be obtained. MPC uses the system model to predict the future output of the system while minimizing the system error, it could potentially provide a faster system response while the accuracy can be improved and simulation results are presented in the next chapter.

CHAPTER 4

ANALYSIS OF RESULTS

4.1 Generator Simulation Results

A speed controller has been implemented for closed loop control of the PMSM so that the motor runs at the commanded reference speed with a fast response and a near zero steady state error. Simulation results of current and voltage in each part of the system is shown, average losses, and efficiency of the drive system can be calculated based on this information.

To demonstrate the operation of the generator, the following simulation scenario is shown. The generator is supplied with constant torque up to its operating speed at 2150 rpm as shown in Figure 4-1.

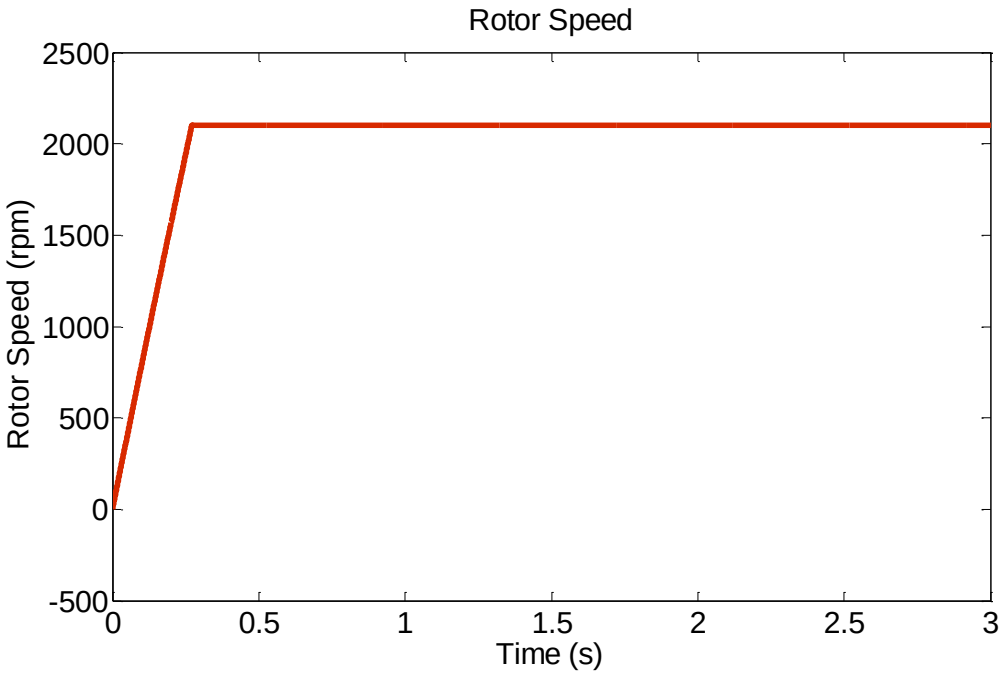

Figure 4-1: Rotor Speed

The rotor speed increases with the torque being applied to the rotor shaft, and the final steady state speed is the same as that of the commanded reference speed.

Figure 4-2 shows the electromagnetic torque of the PMSM. In the generator mode, PMSM converts the electromagnetic torque into voltages and currents. Figure 4-3 shows the voltage and the corresponding d-q component voltages generated by the PMSM.

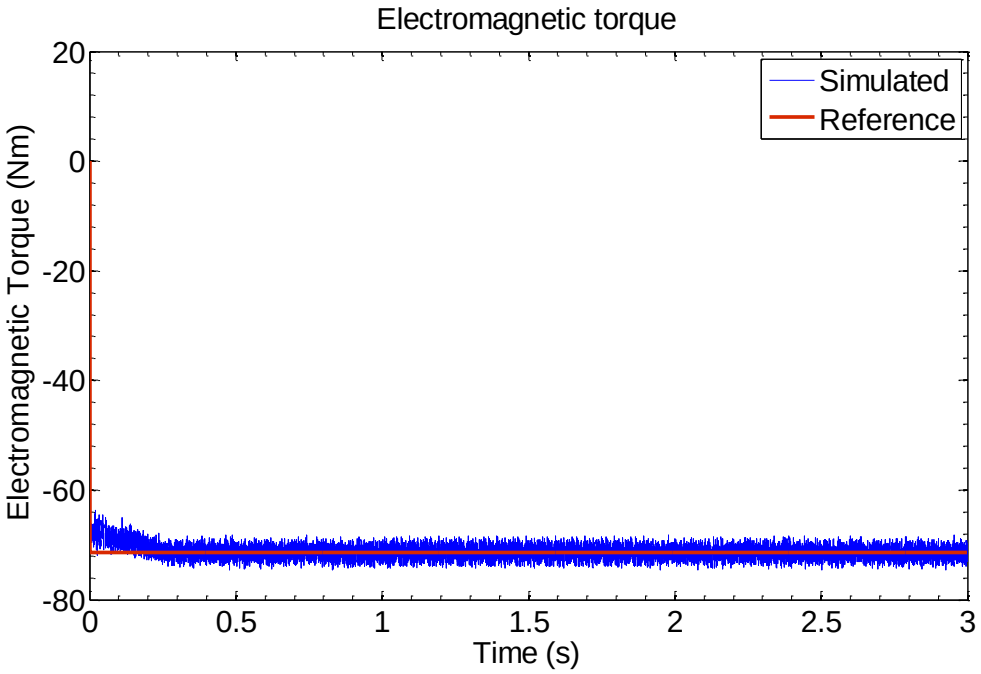

Figure 4-2: Electromagnetic Torque

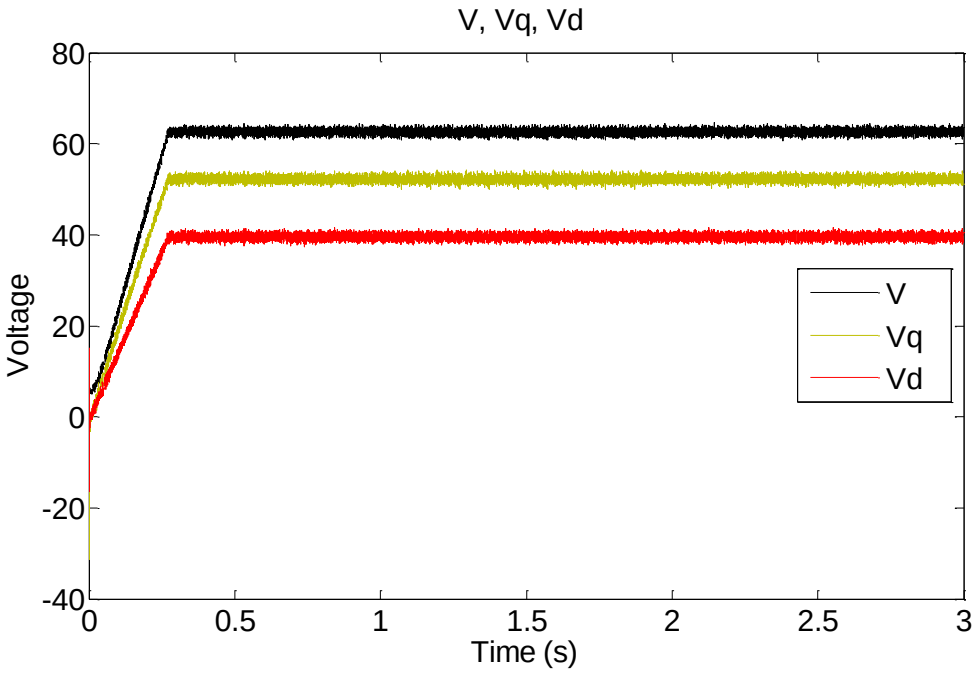

Figure 4-3: Voltage Outputs

Figure 4-4 shows the current and the corresponding d-q component currents generated by the PMSM as a result of the hysteretic current control. The currents are obtained by using Park's reverse transformation. The magnitude of the q axis current is larger than the one of d axis since q axis current is the torque producing current.

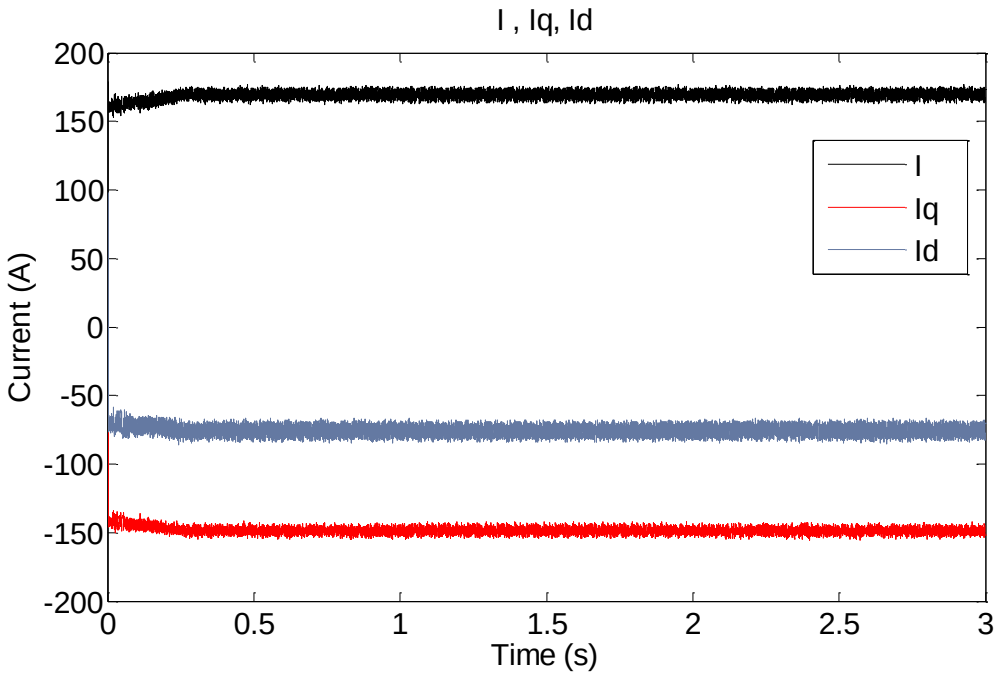

Figure 4-4: Current Outputs

Figure 4-5 shows the electrical power developed by the generator with an approximate value of 16 kW.

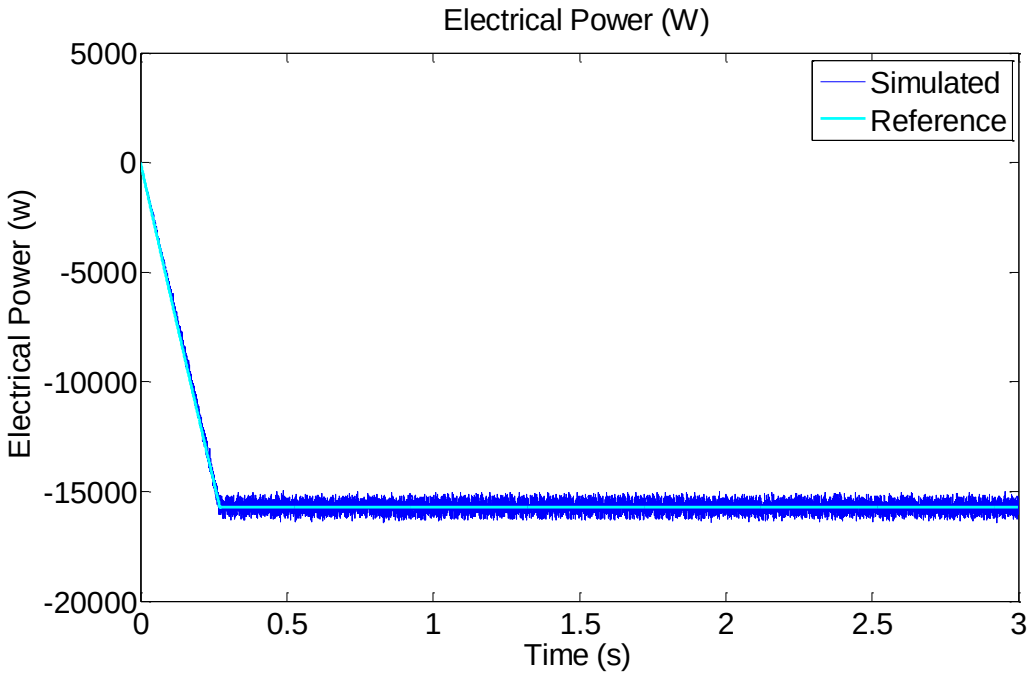

Figure 4-5: Electrical Power

4.2 Emission Model Tuning and Validation

The coefficients in the double Wiebe model (combustion model) were tuned to match the simulated cylinder pressure with the measured one, until a satisfied fit was found. In-cylinder pressure traces have been plotted against the measurement data. For the demonstrated engine operating condition, the engine was running at an engine speed of 1200 rpm; boost with 1.4 bar gauge, 1200bar injection pressure, and 21% of EGR. 50% mass fraction burnt was observed at 368 Degree. A good matching of the peak pressure magnitude and peak pressure rise rate was observed from the predicted and measured traces shown in Figure 4-6.

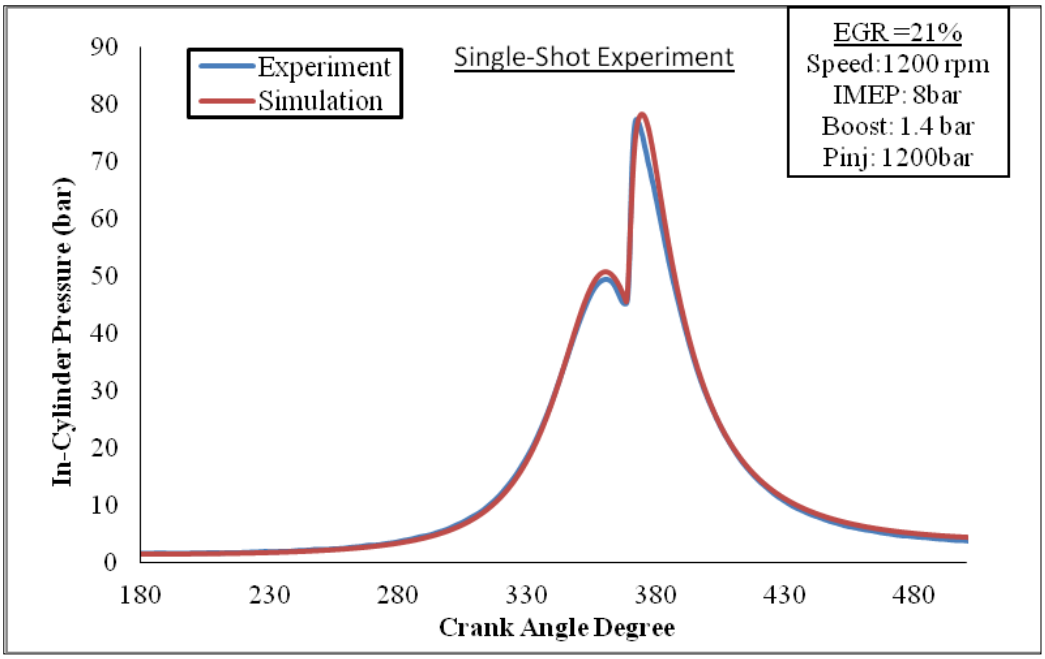

Figure 4-6: Predicted and Measured In-Cylinder Pressure Trace

The predicted cylinder pressure was plotted against measurement data in Figure 4-6. The same pressure traces were used to plot apparent HRR. The predicted HRR data are compared with the measured ones for the same engine operating condition mentioned above, shown in Figure 4-7. A good agreement in trends of simulation and calculated results can be observed.

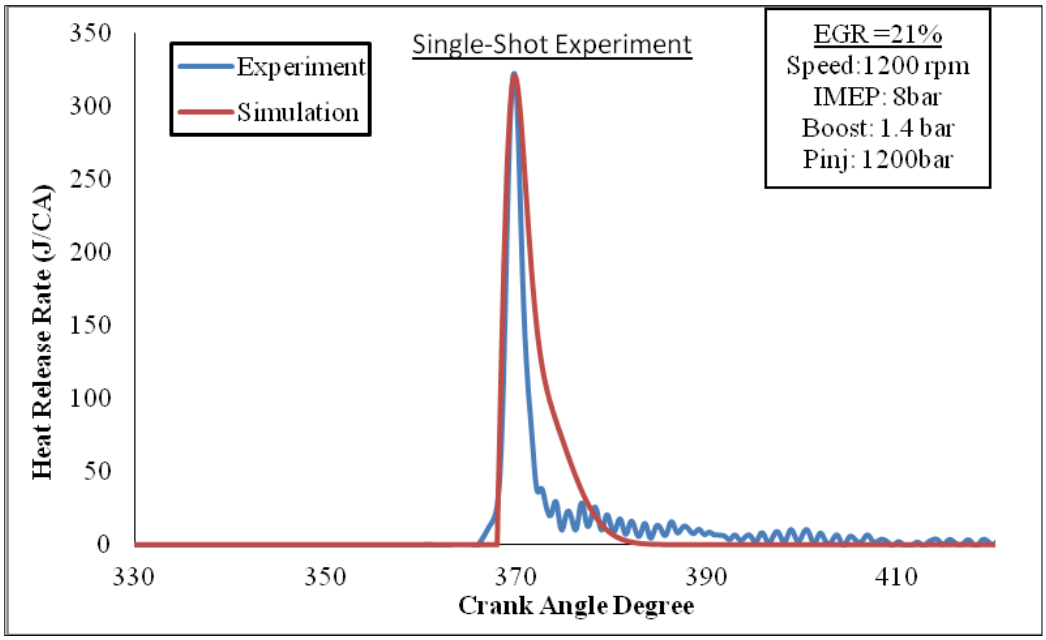

Figure 4-7: Predicted and Calculated HRR Trace

The molar fraction curves for species of O_2, CO_2 and H_2O obtained from the double Wiebe functions blended with EGR effects are shown in Figure 4-8. The molar fraction data were used to predict NOx emission in extended Zeldovich model.

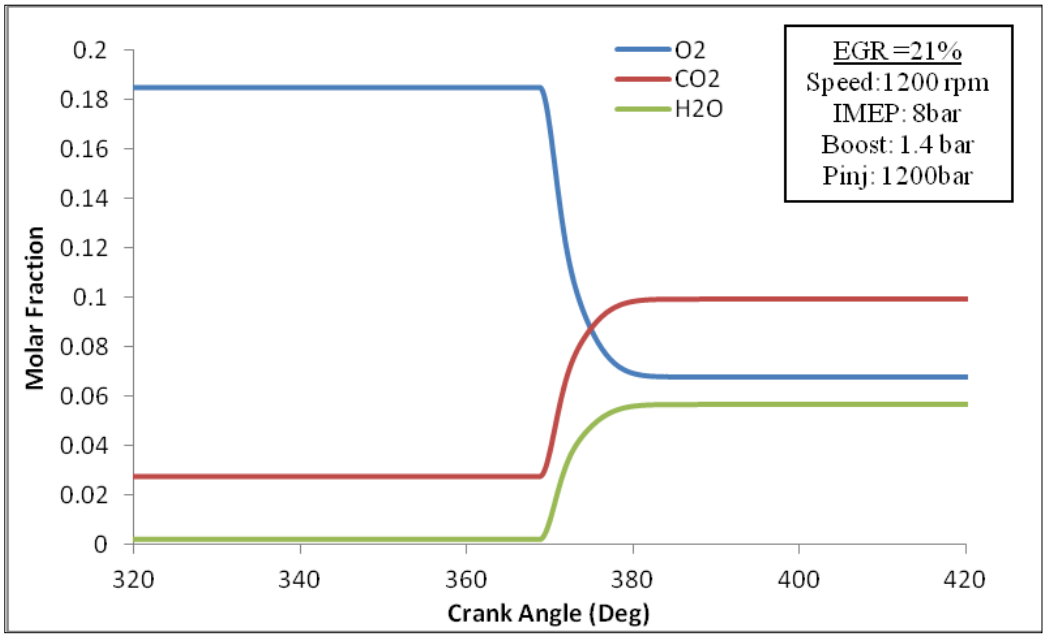

Figure 4-8: Predicted Equilibrium Concentration for Species

The predicted combustion temperature is shown in Figure 4-9. Compared to the combustion with higher EGR of 34% in Figure 4-13, the peak temperature shown in this case is noticeably lower. This lower combustion temperature contributed to a lower NOx emission. This combustion temperature calculation is used for Soot prediction in the Soot model.

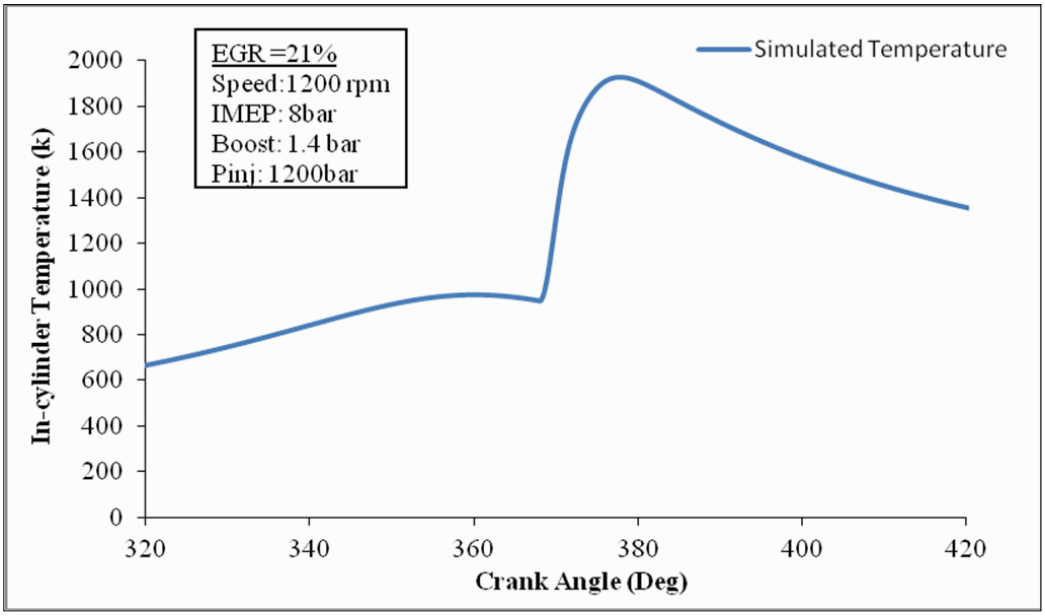

Figure 4-9: Simulated In-Cylinder Temperature

A good match was found for simulated and measured pressure traces at a different engine operating condition with higher EGR and engine load, as can be seen in Figure 4-10. HRR traces were compared for both simulated and measured results as shown in Figure 4-11. A good match of simulated results with experimental results is essential for the emission model.

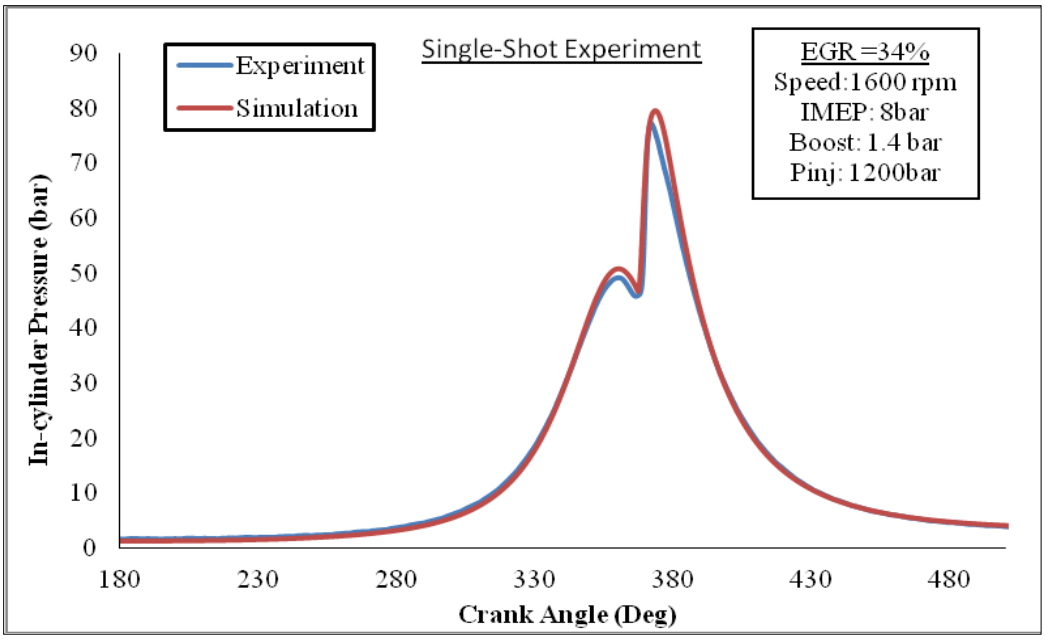

Figure 4-10: Predicted and Measured In-Cylinder Pressure Trace

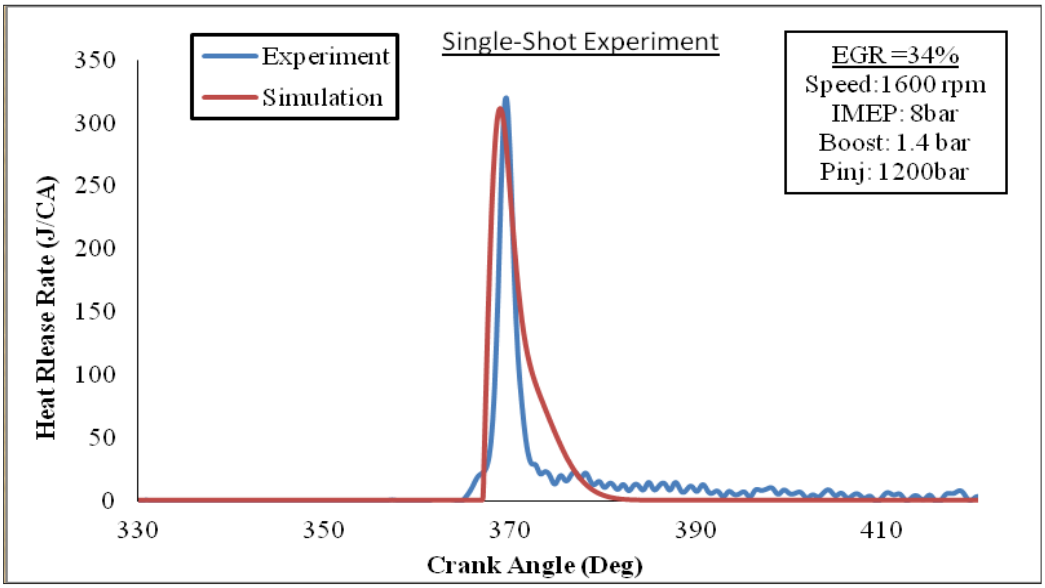

Figure 4-11: Predicted and Calculated HRR Trace

The molar fraction curves for species of O_2, CO_2 and H_2O obtained from the double Wiebe functions blended with higher EGR impacts are shown in Figure 4-12. The oxygen molar concentration decrease significantly compared to the results obtained at a lower

EGR rate. This low oxygen molar concentration helped with NOx reduction.

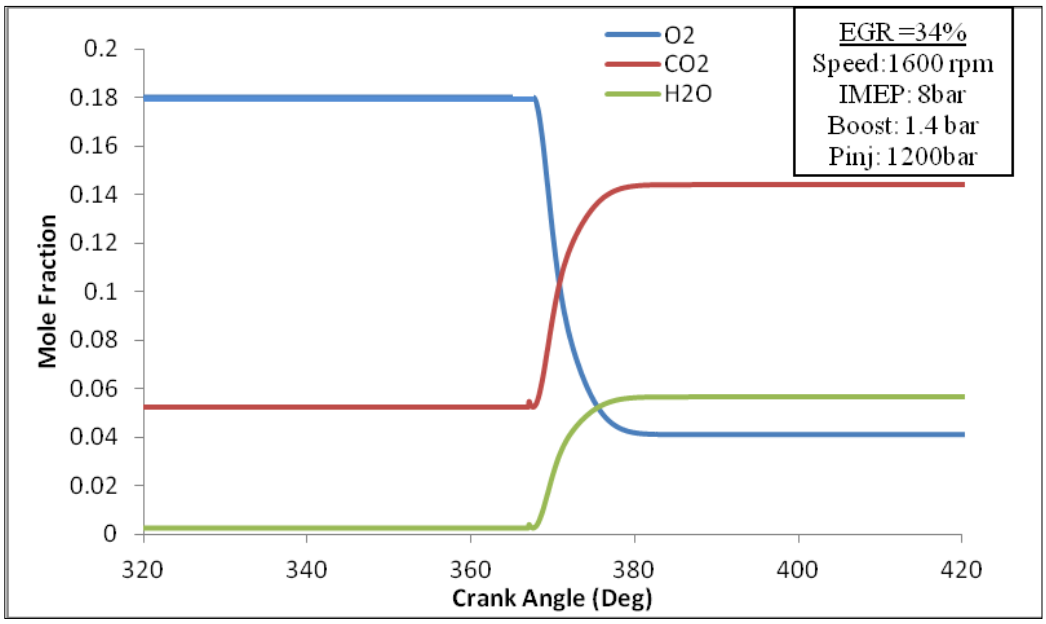

Figure 4-12: Predicted Equilibrium Concentration for Species

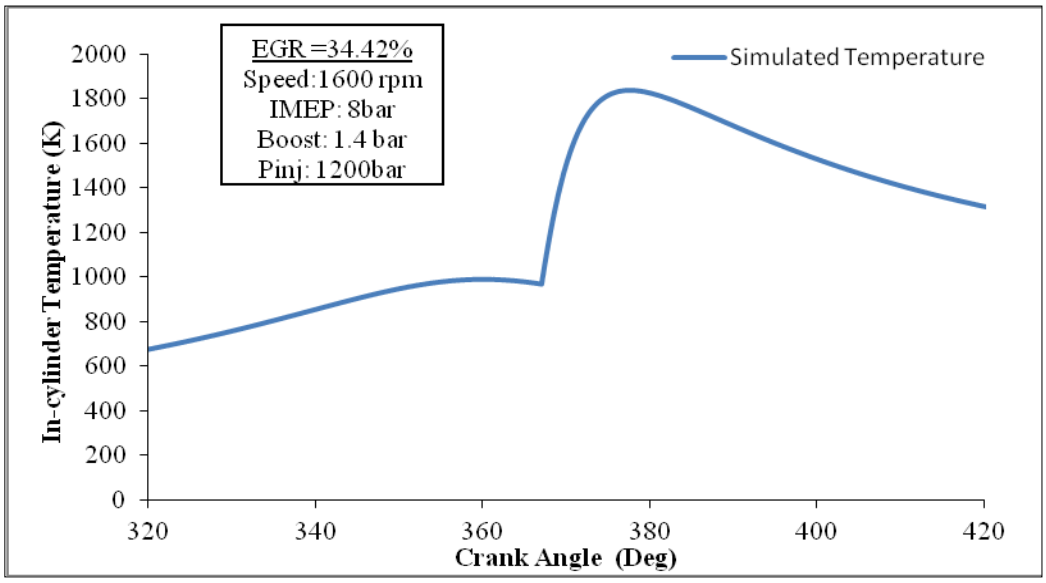

Figure 4-13: Simulated In-Cylinder Temperature

Figure 4-14 shows predicted and measured NOx emissions for the engine speed of 1200 rpm; 1.4 bar gauge boost, and 1200bar injection pressure. The fuel injection rate and

timing were kept the same throughout the experiment. The EGR rate change at this engine load had negligible impact on IMEP. Between measurement and prediction, an acceptable match was found for both in their trend and the quantitative magnitudes for EGR sweeping from 5% to 42%. However, the predicted NOx emission value was over predicted by nearly 10% compared to the measurement.

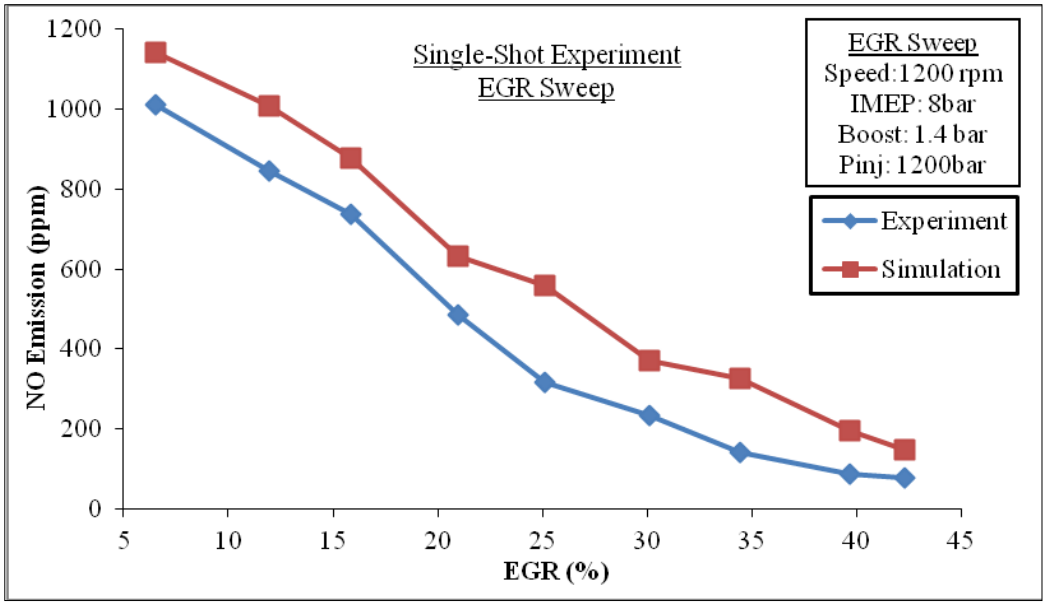

Figure 4-14: Comparison of Predicted and Measured NOx Emission

Combustion temperature traces for different EGR rate and molar fraction of oxygen were used to simulated soot emission. With increased EGR, soot increased as well as expected. Soot emissions are reasonably well predicted by Hiroyasu's two-step soot model in terms of the trends and the magnitudes shown in Figure 4-15.

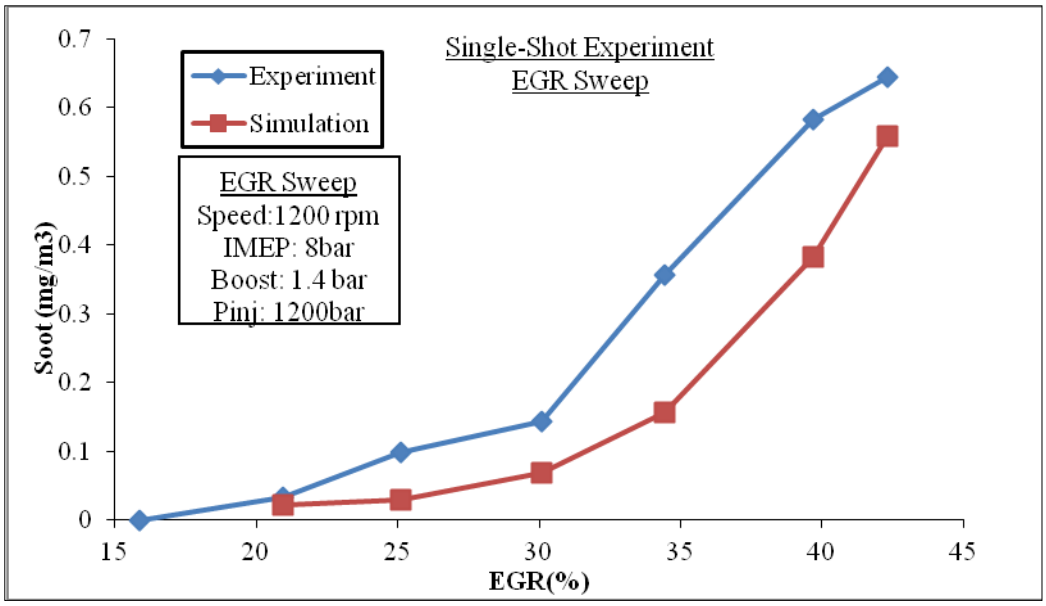

Figure 4-15: Comparison of Predicted and Measured Soot Emission

4.3 Emission Estimation Results

After the emission estimation model was tuned and validated with empirical results, the model was used to predict emission levels for the diesel generator set at its operation points. The amount of EGR that can be applied to the engine is limited by the intake boost level, soot limit and engine load. Figure 4-16 shows the emission estimations at operating point #3, where the engine produces 13 KW at 2150 rpm. For this operation point, the turbocharger generates 1.6 bar abs boost, EGR of 25% can be applied to the engine while NOx is less than 90 ppm and soot is still at an acceptable level at 2.5 FSN.

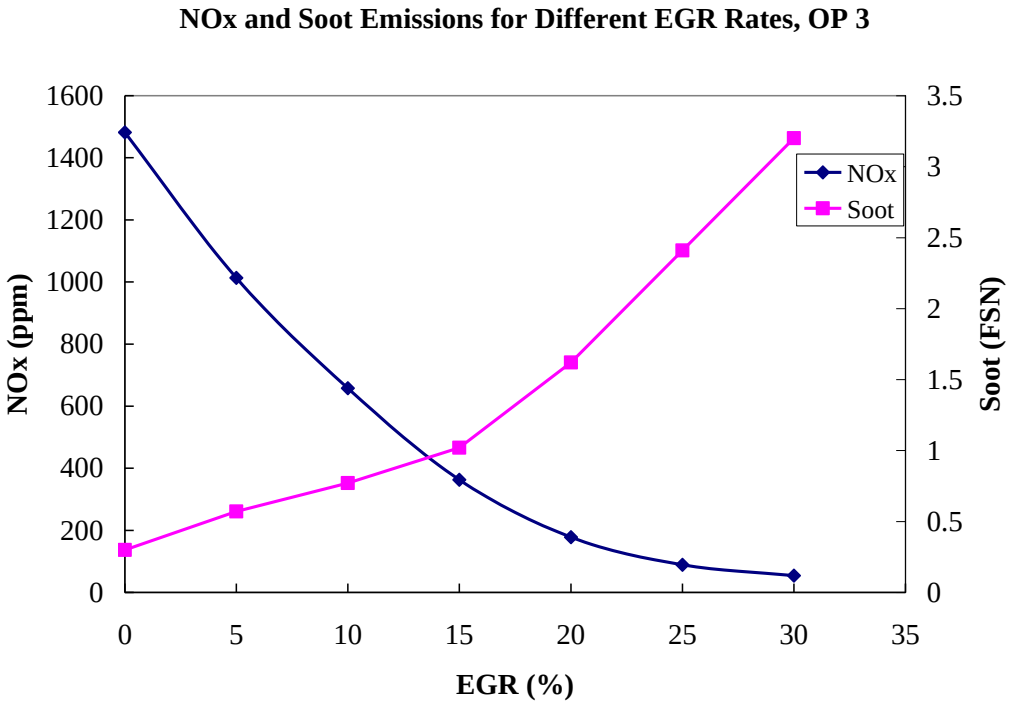

Figure 4-16: NOx and Soot Emissions for Different EGR Rates at Operating Point #3

The corresponding NOx and soot trade-offs with EGR are illustrated in Figure 4-17. Starting with zero EGR, NOx emissions are high and soot emissions are low, while increasing EGR to 15%, NOx was drastically reduced, with 15% of EGR. At low load, the overall air fuel ratio is greater than the high load scenario, and more EGR can be utilized without a high soot penalty. The EGR setpoints for all operating points are estimated and chosen for the engine controller.

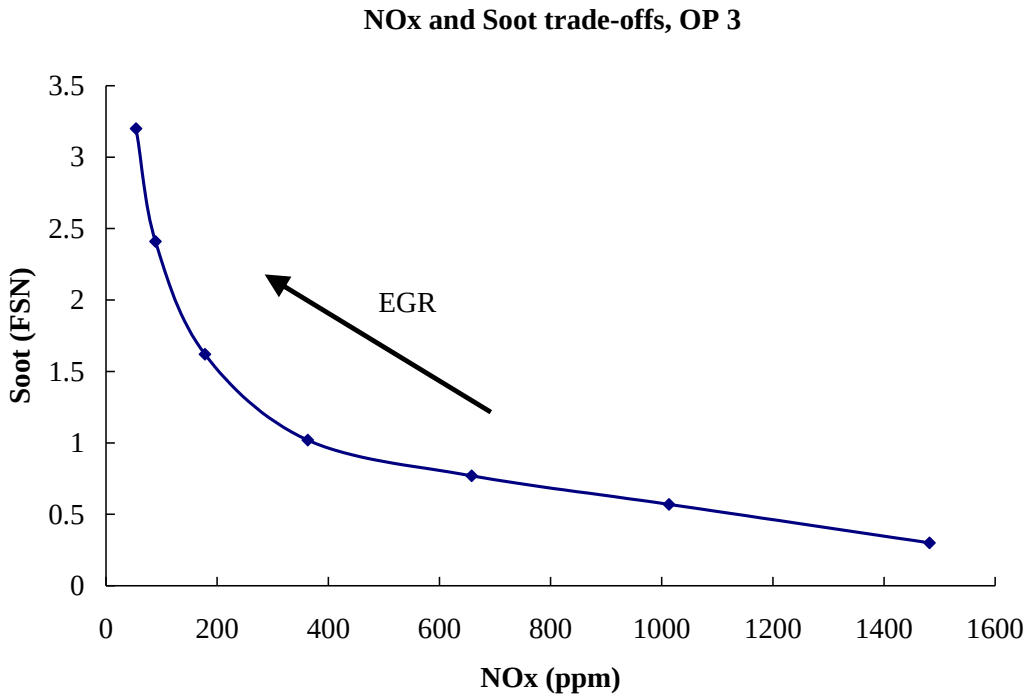

Figure 4-17: NOx and Soot Trade-off at Operating Point #3

4.4 Power Control via Model Predictive Control

The controller was implemented to ensure it has quick and robust control over the engine speed. It was required to closely follow the reference trajectory and provide a near zero stationary error, less than 1% of the reference value. To test the effectiveness of MPC for the engine generator set, a step change of 25 rpm was introduced at 1 second, actual engine speed should follow a reference signal, and results for engine operating point 1, 5 and 8 are shown. The variable for MPC to manipulate is engine fuel injection rate, the response towards the engine speed change is shown as well.

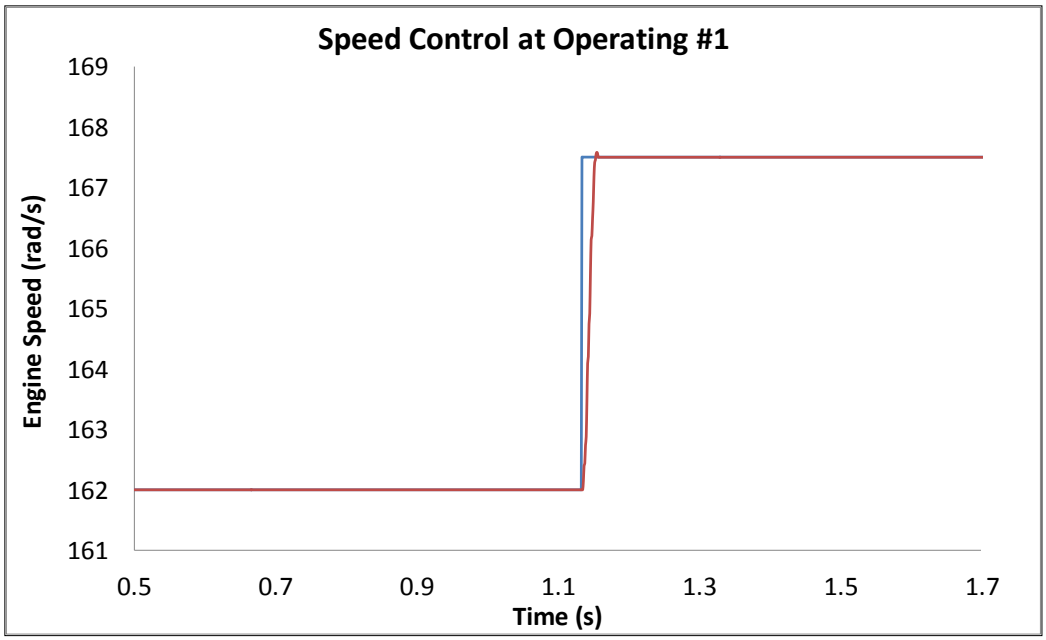

Figure 4-18: Engine Speed Control by MPC at Operating Point #1

Figure 4-18 shows the control over the engine speed at operating point #1, achieved using the MPC controller. At this operating point, the engine generator set is running at 167.4 rad/s (1600 rpm) and produces 7 KW power. It is observed that the engine speed is able to follow the reference, given a minimum overshoot with a near zero stationary error 0.1 second later. Figure 4-19 shows the change in fuel injection rate which is the manipulate variable.

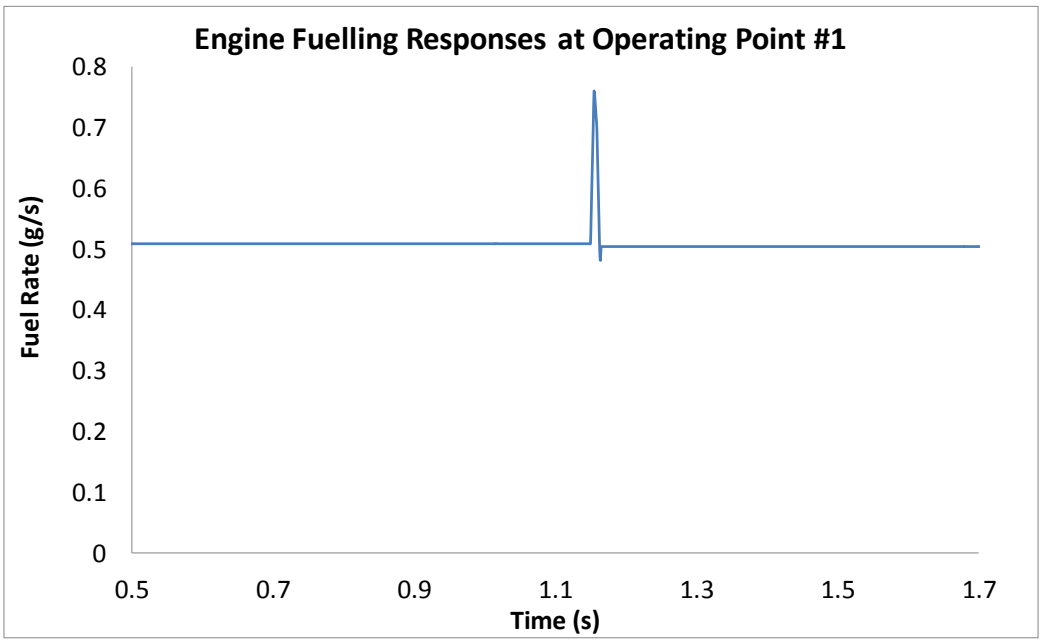

Figure 4-19: Engine Fuelling Responses at Operating Point #1

The step of the manipulate variable was set to 0.015 seconds, the simulation time step is set at 0.001 seconds to ensure the desired system responses. Fuel rates compensate the sudden change of engine speed by increasing its value to provide more torque output, once the reference engine has been met, the fuel injection stabilized. Figure 4-20 shows the corresponding voltage change for the generator.

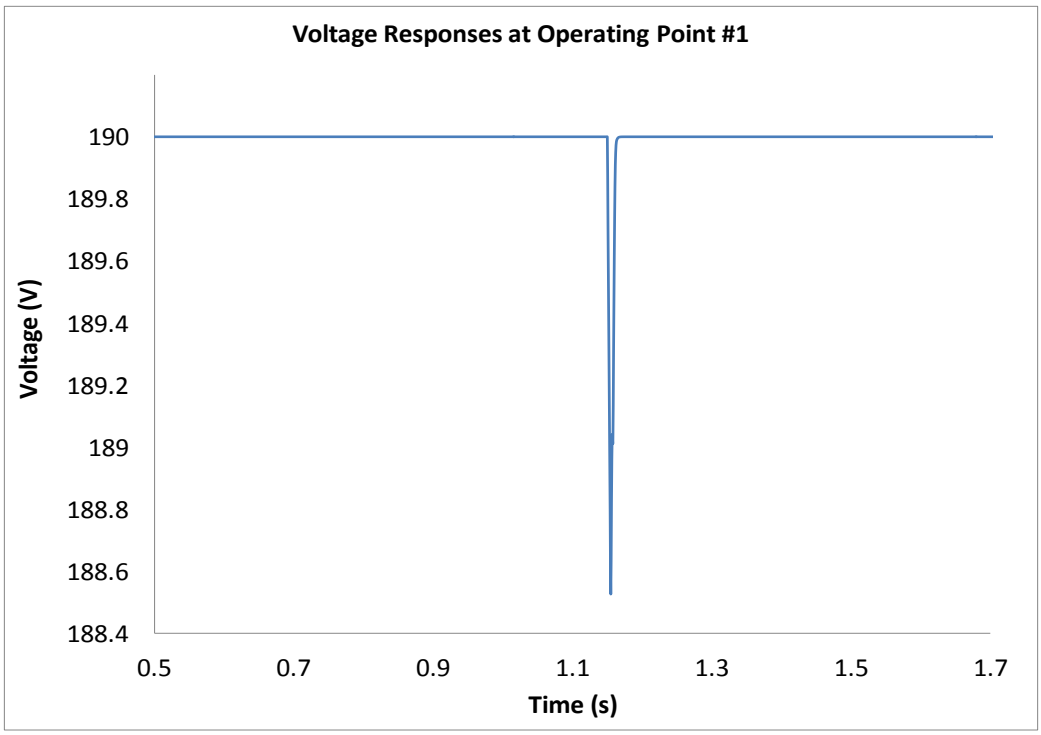

Figure 4-20: Generator Voltage Responses at Operating Point #1

Figure 4-21 shows the corresponding q-axis current change for the generator during the speed transition, the q-axis current oscillated fast as the engine speed quickly following up with the reference one.

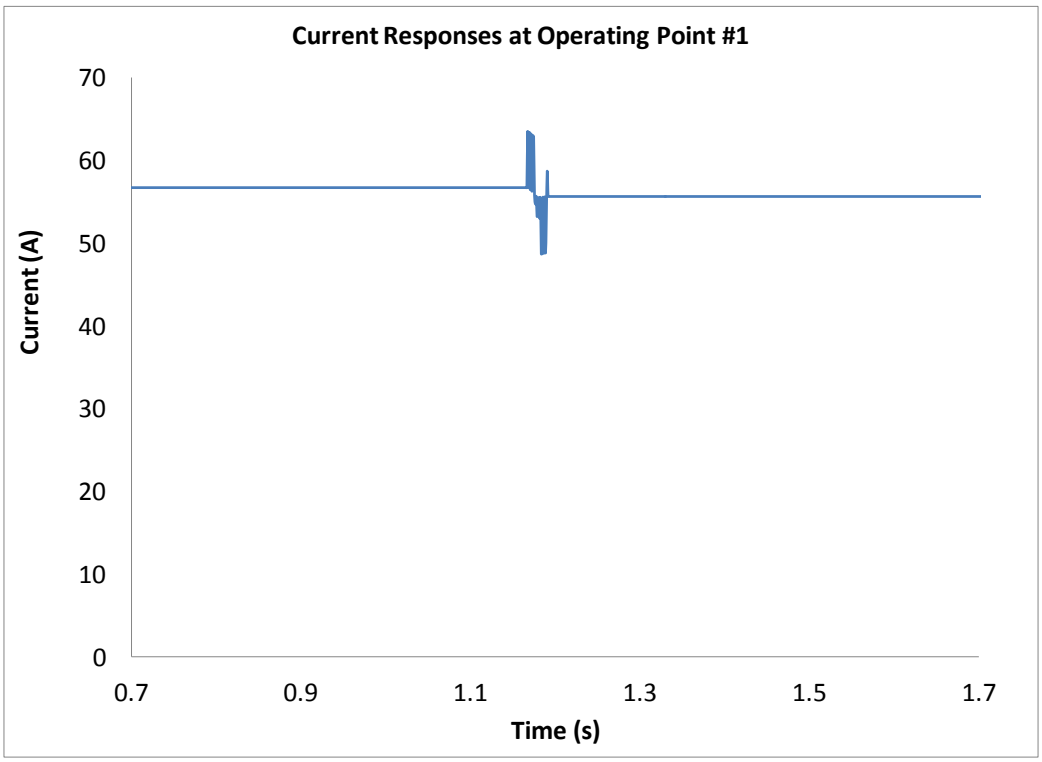

Figure 4-21: Generator Current Responses at Operating Point #1

Figure 4-22 and Figure 4-23 demonstrates the MPC performance at engine operating point 5. The nominal engine operating speed is at 256.4 rad/s (2450 rpm), at 2.5 seconds a step change of reference speed was introduced with the magnitude of 4.5 rad/s. Figure 4-22 shows that the system was able to closely follow the reference trajectory with minimal overshoot and a near zero steady state error.

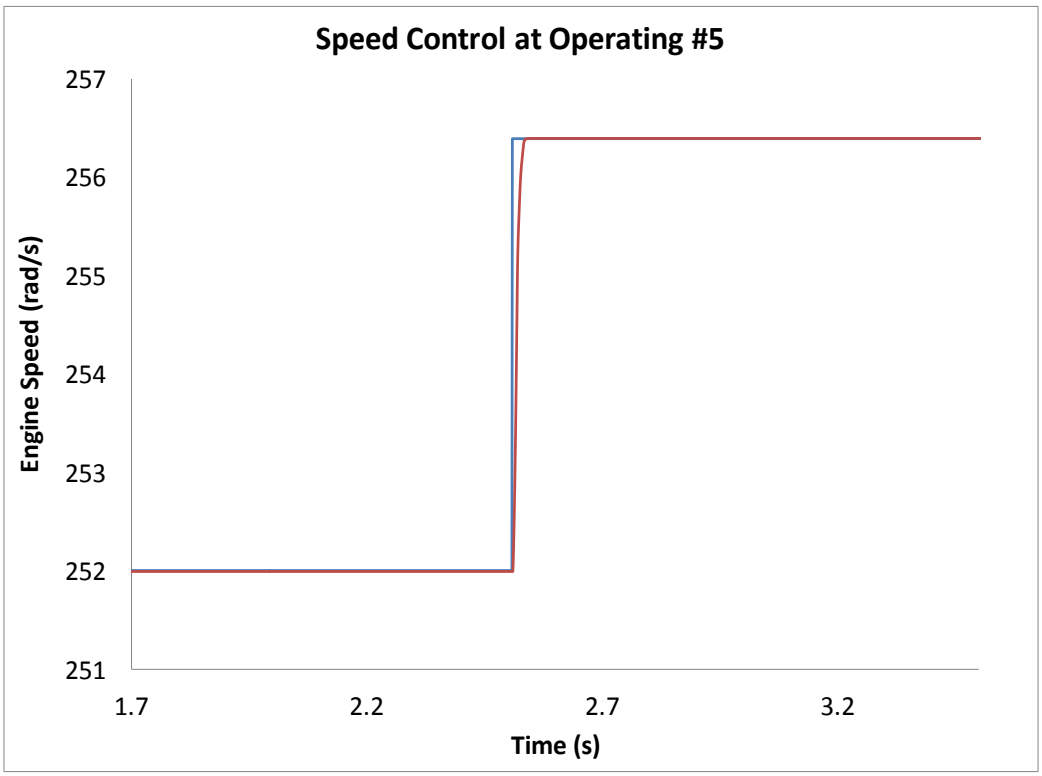

Figure 4-22: Engine Speed Control at Operating Point #5

Figure 4-23 shows the fuelling changes for the engine to accommodate the step reference speed change. By quickly adjusting the fuel injection rate to the engine from 1.306 g/s to 1.44 g/s, the engine was outputting more torque instantly to spin up the system, therefore, the desired reference speed was closely followed.

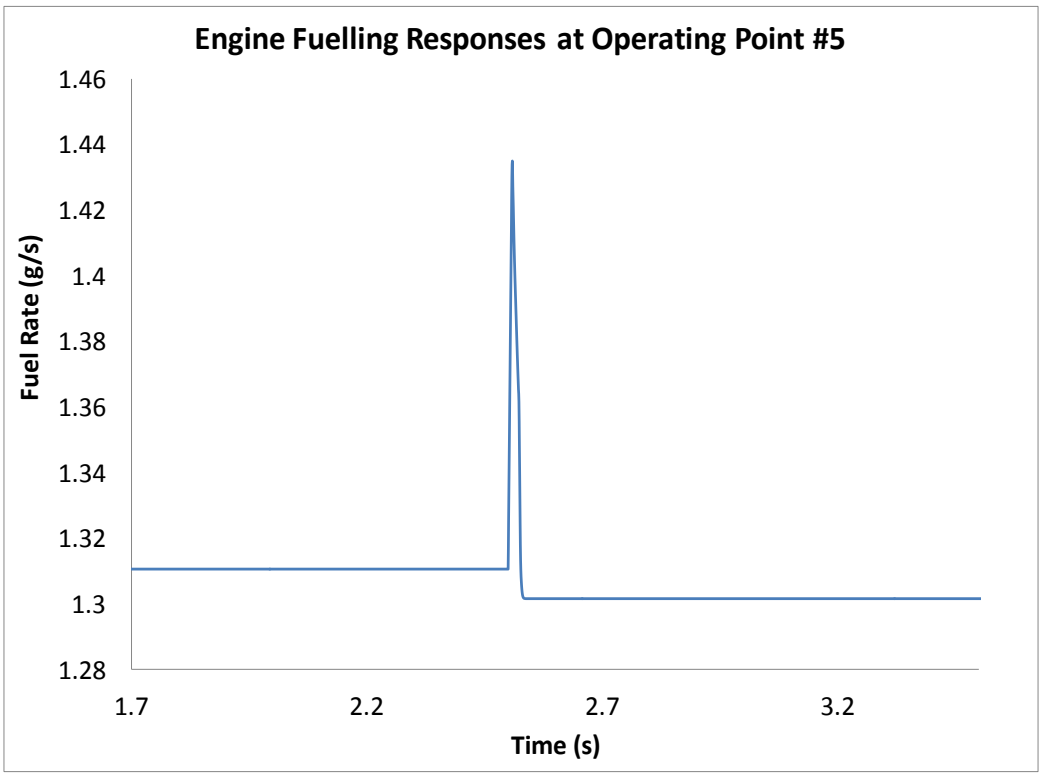

Figure 4-23: Engine Fuelling Responses at Operating Point #5

The simulation study demonstrates the controller's ability to track a reference trajectory with quick response while achieving efficient engine operation.

CHAPTER 5

CONCLUSION AND RECOMMENDATIONS

5.1 Conclusions

In a SHEV, the fuel economy and emissions heavily depend on the operation of the engine generator set, so it is crucial to have the power and emissions under control. A diesel engine generator set model was firstly proposed as a platform to perform the power control and predict exhaust emissions. The engine model was derived from empirical test results. A PMSM was modeled as a generator based on first principles. Furthermore, operation points to achieve best fuel economy were identified and chosen, variable speed operation of the engine-generator set is enabled in accordance with the vehicle power demand to improve the fuel efficiency and reduce emission. EGR effects for diesel combustion was modeled, EGR impacts on NOx and soot emissions were simulated for each of the engine generator set operating point, optimal amount of EGR was determined based on the trade-off between NOx and soot. MPC was applied for performing the power control of the diesel engine generator set at each operating point. The simulation results demonstrated that the control's capability to track the reference, effective power control was shown. Power control of the diesel engine generator set was subject to emission constrains for a SHEV in charge sustaining mode was achieved.

5.2 Recommendations

The following recommendations are made for further researches:

From the modeling aspect, future work may concentrate on model validation using the hardware-in-the-loop (HIL) setup. In the HIL setup, it is desired to have the diesel engine and generator setup, so that system efficiency and emissions can be obtained from empirical results for further model tuning and result validation.

An overall vehicle dynamics model with aerodynamics, tires, frictions and weights is required to test and validate the developed engine generator set control. This model can be used as a platform to run different standard test cycles, fuel efficiency and emissions can be compared to different control strategies.

A model based EGR control can be developed to enable a close loop control of the emission levels by achieving an optimal EGR amount for each operating points. The controller needs to ensure EGR setpoints can be quickly reached and the control of EGR control is robust against disturbances.

REFERENCES

1. W. Addy Majewski., “Diesel Emission Control”, 2007
2. EPA, Automobiles and Highway Trucks and Buses Emission Standards 2010, Dieselnet, “Emission Standards” – http://www.dieselnet.com/standards/us/ accessed 2011
3. European Union Cars and Light Trucks Emission Standards, Dieselnet
4. U.S. Energy Information Administration, E.I. 2007, http://www.eia.doe.gov/neic/ quickfacts/quickoil.html, accessed 2011
5. U.S. Energy Information Administration. The Annual Energy Review. Technical report, 2006, http://www.eia.doe.gov/aer/
6. U.S EPA National Program to Reduce Greenhouse Gases and Improve Fuel Economy for Cars and Trucks, http://www.epa.gov/otaq/climate/regulations/420 f10014.htm
7. European Parliament, “Reducing CO2 emission form new cars” 2006 Progress report on the car industry’s voluntary commitment, September 2007.
8. P. K. Chiang, “Two-Mode Urban Transit Hybrid Bus In-Use Fuel Economy Results From 20 Million Fleet Miles”. 2007, SAE.
9. Diesels Market Share in Western European for Passenger Car Market http://www.greencarcongress.com/2010/02/acea-20100204.html
10. J. E. Kirwan, M. Shost, G. Roth, "3-Cylinder Turbocharged Gasoline Direct Injection: A High Value Solution for Low CO2 and NOx Emissions" SAE 2010-01-0590

11. M. Ehsani, K. M. Rahaman, H. A. Toliyat, "Propulsion System Design of Electric and Hybrid Vehicle", IEEE Trans. on Ind. Elec., Vol144, NO 1, 1997
12. A. Brahma, Y. Guezennec, and G. Rizzoni, Optimal Energy Management in Series Hybrid Electric Vehicle, Proc. Of American Control Conference, Chicago, 2000.
13. B. K. Powell, and T. E. Pilutti, , A Range Extender Hybrid Electric Vehicle Dynamic Model, Proc. of the 33rd Conference on Decision and Control, Florida, pp. 2736-2741, 1994.
14. M. Ehsani, Y. Gao, S.E. Gay and A. Emadi, "Modern Electric, Hybrid Electric, and Fuel Cell Vehicles: Fundamentals, Theory and Design", CRC, 2005.
15. J. Heywood B, Internal Combustion Engine Fundamentals, McGraw-Hill, New York, 1988
16. J. H. Lee, S. H. Lee, and S. K. Sul, " Variable-Speed Engine Generator with Supercapacitor: Isolated Power Generation System and Fuel Efficiency," IEEE Trans. Industrial Application, Vol. 45, No. 6, Nov. 2009
17. H. Yoo, S. K. Sul and Y. Park, "System Integration and Power-Flow Management for a Series Hybrid Electric Vehicle Using Supercapacitors and Batteries," IEEE Trans. Industrial Application, Vol. 44, No. 1, Jan. 2008
18. Diesel Oxidation Catalyst, Johnson Matthey, http://ect.jmcatalysts.com/pdfs-library/jm_sec_data_doc_012809m.pdf, accessed on 2011
19. M. Zheng, , G. T. Reader, , and G. J. Hawley,; “Diesel Engine Exhaust Gas Recirculation – a Review on Advanced and Novel Concepts”, Journal of Energy

Conversion and Management, Elsevier Science Ltd., Vol. 45/6, 2004, pp. 883-900.

20. M. Fathi, R. K. Saray, M. Pourfallah, J. Kheyrollahi, G. Javadirad, "EGR and Intake Charge Temperature Effects on Dual-Fuel HCCI Combustion and Emissions Characteristics" SAE 2011-24-0050, 2011
21. U. Asad, , M. Zheng, , "Efficacy of EGR and Boost in Single-Injection Enabled Low Temperature Combustion", SAE 2009-01-1126
22. J.I. Ramos. Internal Combustion Engine Modeling. Hemisphere Publishing Corporation, 1989
23. H. Kim, N. Sung, "Combustion and Emission Modeling for a Direct Injection Diesel Engine", SAE 2004-01-0104, 2004
24. A.J. Truscott and A.F. Cotta. Dynamix Diesel Engine System Model for Fault Detection: Therory of Model. Ricardo Consulting Engineering Ltd, 1999
25. S. Abuelsamid, "Frankfurt 2007: Smart ForTwo Micro Hybrid Launches". GreenAutoblog. 2007
26. P. B. Sharer, A. Rousseau, D. Karbowski and S. Pagerit, "Plug-in Hybrid Electric Vehicle Control Strategy: Comparison between EV and Charge-Depleting Options." SAE 2008-01-0460, 2008
27. K. Rajashekara, S.S. Williamson and S. M. Lukic, “Topological Overview of Hybrid Electric and Fuel Cell Vehicular Power System Architectures and Configurations,” IEEE Tran. On Vehicular Technology, Vol. 54, No. 3, 2005

28. K. L. Shi, Hassan Kojori and Bin Wu, "High-Performance Sensorless PMSM Drive With Extended Kalman Filter," SAE TECHNICAL PAPER, 2002-01-3253, 2002
29. J. Leuchter, P. Bauer, V. Rerucha, and Z. Krupka, “Dynamic Behaviour Identification of Electrical Gen-Set,” in Proc. Int. Power Electron. Motion Control Conf.
30. I. Jadric, D. Borojevic, and M. Jadric, “Modeling and Control of a Synchronous Generator with an Active DC Load,” IEEE Trans. Power Electronics, Vol. 15, No. 2, pp. 303–311, Mar. 2000
31. P. Pillay and R. Krishnan, "Modeling of Permanent Magnet Motor Drives," Industrial Electronics, IEEE Transactions on, vol. 35, 1988.
32. C. M. Ong, Dynamic Simulation of Electric Machinery using Matlab/Simulink, Prentice Hall, 1998.
33. M. H. Kao, J. J. Moskwa, “Turbocharged Diesel Engine Modeling for Nonlinear Engine Control and State Estimation,” ASME Journal of Dynamic Systems, Measurement, and Control, Vol. 117, Mar. 1995.
34. M. Andersson, B. Johansson, A. Hultqvist, C. Nohre, "Real Time NOx Model for Conventional and Partially Premixed Diesel Combustion" SAE 2006-01-0195
35. A. Westlund, H.Ek Angstrom, "Fast Physical Prediction of NO and Soot in Diesel Engines" SAE 2009-01-1121, 2009
36. J. Kwon, J. Seo, D. Lee and K. Y. Huh, "Zero-Dimensional Simulation of Diesel Engine Combustion and Emissions Based on CMC Model and Skeletal Reaction Mechanism", SAE 2011-01-0845, 2011

37. T. V. Johnson, "Review of Diesel Emissions and Control"' SAE Technical Paper, 2010-01-0301, 2010
38. H. Yasar, H.S. Soyhan, Walmsley, B. Head, C. Sorusbay "Double-Wiebe Function: An approach for single-zone HCCI engine modeling", Applied Thermal Engineering 28, 2008
39. U. Asad, M. Zheng, "Real-time Heat Release Analysis for Model-based Control of Diesel Combustion", SAE 2008-01-1000
40. H. Hiroyasu "Diesel Engine Combustion and its Modeling". Proceedings of 1st International Symposium on Diagnostics and Modeling of Combustion in internal Combustion Engines. Tokyo, Japan, April 1985, p. 53 – 75
41. G.A. Lavoie, J.B. Heywood and J.C. Keck (1970). Experimental and Theoretical Study of Nitric Oxide Formation in Internal Combustion Engines. Combustion Science and Technology, 1.
42. F. Payri, Jean Arregle, J. J. Lopez, and E. Mocholi; "Diesel NOx Modeling with a Reduction Mechanism for the Initial NOx Coming from EGR or Re-entrained Burned Gases" , SAE 2008-01-1188, 2008
43. C. Wilhelmsson, P. Tunestal and B. Johansson, "A Physical Two-Zone NOx Model Intended for Embedded Implementation," SAE 2009
44. H. Hiroyasu, T. Kadota, and M. Arai, "Development and Use of a Spray Combustion Modeling to Predict Diesel Engine Efficiency and Pollutant Emissions," Bull. JSME, Vol. 26, No. 214,
45. C. Alkidas, "Relationships between smoke measurements and particulate measurements," SAE 840412, 1984.

46. B. Saerens, M. Diehl, J. Swevers and E. V. Bulck, "Model Predictive Control of Automotive Powertrains - First Experimental Results," in 47th IEEE Conference on Decision and Control Cancun, Mexico, Dec. 9-11, 2008
47. C. Edberg. “Control of Systems with Constraints.” Master Degree Thesis, Royal Institute of Technology, Stockholm 2004.
48. D. Liu, L. Dou, J. Chen, Y, Xia, "Hybrid model predictive control for speed control of permanent magnet synchronous motor with saturation," Journal of Control Theory Application, 2011 9 (2) 251–255
49. E. F. Camacho, and C. Bordons , “Model predictive control” Springer, London, ISBN 3-540-76241-8-1999
50. G. F. Franklin, D. J. Powell, and M. L. Workman, Digital control of dynamic systems (3rd Edition), Prentice Hall, 1997
51. P. Ortner, P. Langthaler, J. V. G. Ortiz, and L. del Re, “MPC for a diesel engine air path using an explicit approach for constraint systems,” in Proc. IEEE International Conference on Control Applications, Munich, Germany, 2006
52. K. S. Low, and H. Zhuang , “Robost Model predictive control and observer for direct drive applications,” IEEE Trans. Power Electron. 15:1018-1028, 2000.
53. N. Gould and P. L. Toint. “Preprocessing for quadratic programming.” Math. Programming, Series B, Vol.100, pp. 95-132, 2004
54. B.W. Bequette “Process control modelling design and simulation” Prentice Hall Edition, 2004
55. M. Morari and N. Lawrence Ricker “Model predictive control toolbox user’s guide”, 2011

VITA AUCTORIS

NAME:	Xiaoxi Zhang
PLACE OF BIRTH:	Hubei, China
YEAR OF BIRTH:	1981
EDUCATION:	McMaster University, Hamilton, Ontario
	2003-2007, B.Eng
	University of Windsor, Windsor, Ontario
	2003-2007, M.Eng
	University of Windsor, Windsor, Ontario
	2009-2012, M.A.Sc